AD-A071 765 TECHNION - ISRAEL INST OF TECH HAIFA DEPT OF AERONAU--ETC F/G 20/4
STUDIES OF NON-LINEAR AERODYNAMIC CHARACTERISTICS OF FINNED SLE--ETC(U)
NOV 78 J ROM, D ALMOSNINO DA-ERO-78-G-021
UNCLASSIFIED TAE-349 NL

| OF |
AD
A071765

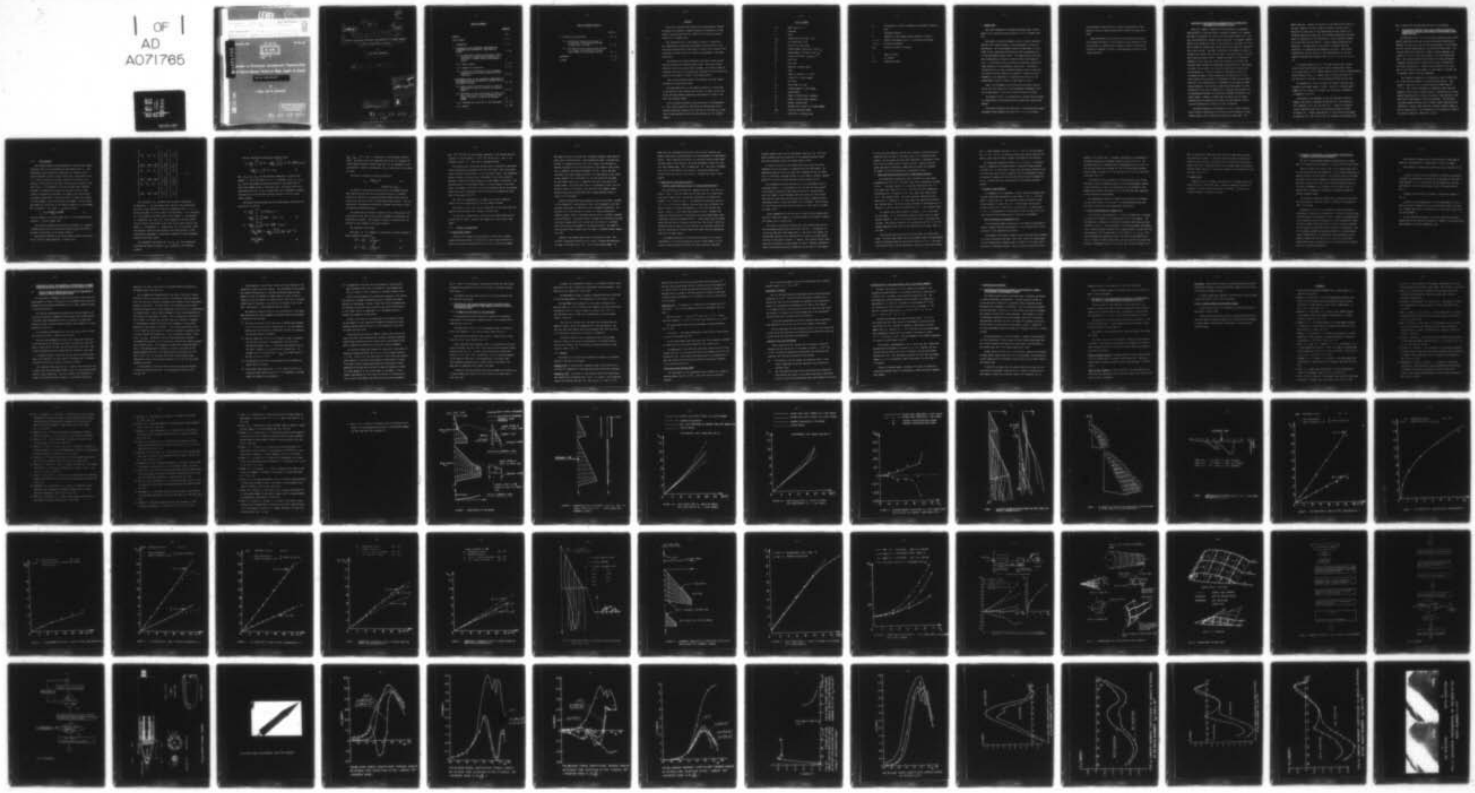

END
DATE
FILMED
8-79
DDC

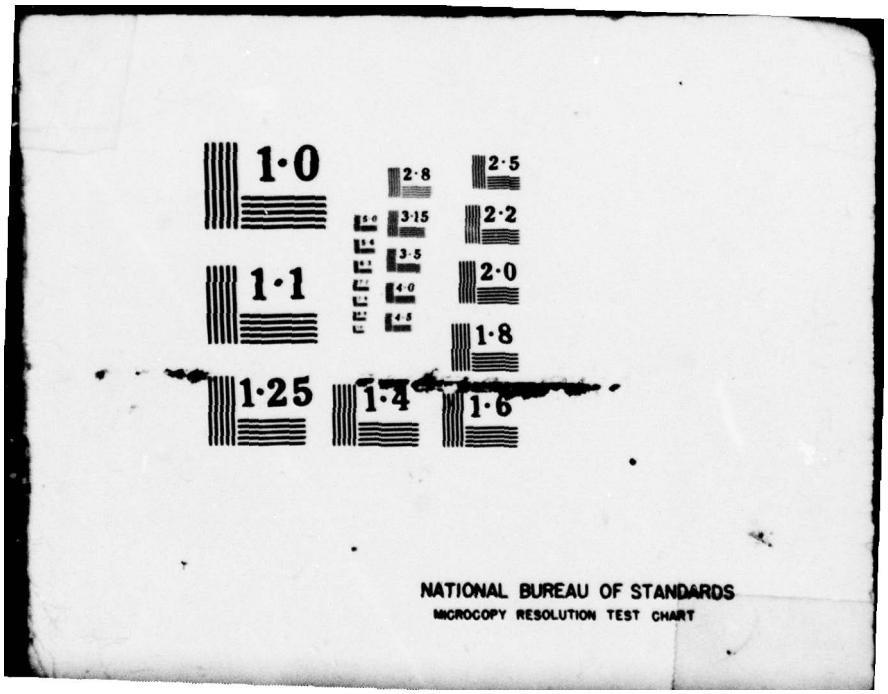
1·0
1·1
1·25
1·4
1·6
1·8
2·0
2·2
2·5
2·8
3·15
3·5
NATIONAL BUREAU OF STANDARDS
MICROCOPY RESOLUTION TEST CHART

November, 1978

TAE No. 349

Studies of Non-Linear Aerodynamic Characteristics of Finned Slender Bodies at High Angles of Attack

Grant No. DAERO-78-G-021

by

J. Rom and D. Almosnino

(1)

(12) 80p.

(11) NOVEMBER 1978

(14) TAE-349

(9) Rept. for Oct 77-Nov 78,

(6) STUDIES OF NON-LINEAR AERODYNAMIC CHARACTERISTICS OF FINNED SLENDER BODIES AT HIGH ANGLES OF ATTACK.

by

(10) J. ROM and D. ALMOSNINO

(15) DA-ERO-78-G-021

TABLE OF CONTENTS

TABLE OF CONTENTS (CONT'D).

ABSTRACT

This report describes both theoretical and experimental research performed on the subject of slender wing-body configurations at high angles of attack, under Grant No. DAERO-78-G-021 during the period October 1977 - November 1978.

The theoretical part of the research consists of a method for the computations of longitudinal aerodynamic characteristics of complex wing configurations at high angles of attack, and in subsonic flow including non-linear vortex lift caused by leading-edge or side-edge separations.

The modified vortex method developed can handle closely coupled canard configurations, dihedral angles, flaps, "saw-tooth",strakes, elevators, as well as, ground effect problems. An outline is made for including a body and for calculating the influence of vortices shed from bodies at high angles of attack, in the present method.

Some of the calculated results are presented, and those compare favourably with experimental data.

The experimental part of the research consists of a study made on the effects of jets injected near the nose of a body, on the side forces and yawing moments appearing at high angles of attack at subsonic and transonic speeds.

One of the main conclusions from the results of the experiments is that a great reduction of side-force and yawing moment can be achieved using small amounts of air injection by this method. Further study is need especially within the high subsonic and the transonic regions.

LIST OF SYMBOLS

AR	aspect ratio, b^2/S
b	wing span
C	chord
C_{D_i}	induced drag coefficient D/qS
C_L	lift coefficient, L/qS
C_ℓ	section lift coefficient
C_M	pitching moment coefficient M/qS C_{ref}
C_n	yawing moment coefficient N/qS C_{ref}
C_μ	blowing coefficient $\dot{m}_j u_j / \frac{1}{2} \rho_\infty U^2 S$
C_y	side force
D	drag force
H	geometric influence matrix
i	index
j	index (or subscript for "jet")
K	strength of a vortex segment
L	lift force
$\dot{m}_j$	nozzle mass flow rate
M	pitching moment, or Mach number
N	yawing moment
N_c	number of subdivisions, chordwise
N_s	number of subdivisions, spanwise
q	dynamic pressure, $\frac{1}{2}\rho V^2$
r	distance from a point to a vortex segment
Re_c	cross flow Reynolds number
S	wing area, or reference area

u_j	theoretical jet velocity (assuming fully expanded isentropic flow)
U	freestream velocity
$\hat{w}$	component of free stream velocity normal to a surface
u, v, w	velocity disturbances in x, y, z directions accordingly
x, y, z	Cartesian coordinates
X_{cp}	position of center of pressure
α	angle of attack
ρ	air density
ϕ, θ	geometrical angles

1. INTRODUCTION

This report summarizes the research performed under Grant No. DAERO-78-G-021 during the period October 1st 1977 to November 30th 1978.

High angle of attack performance is one of the most important regions in the flight envelope of the new generation of aircraft and missiles. The flow phenomena involved in high angle of attack flight is very complicated and therefore a most challenging area for the aerodynamic research effort. The analysis may involve complex configurations of wings and bodies on which flow separation occur. In such flows strong vortices may be generated causing non-linear behaviour of the aerodynamic coefficients. Furthermore, configurations with strong interaction between closely coupled lifting surfaces and their wakes may be analyzed. Another well known phenomenon is the appearance of relatively large side force and yawing moments acting on bodies at high angles of attack.

Some of the phenomena involve strong viscous effects such as the not yet fully understood "vortex break-down" phenomenon, occuring at high angles of attack when strong vortices are involved.

The present efforts of aerodynamicists to analyze these problems are concentrated on developing theoretical models and computational methods.

This report describes the application of the computational method developed by Rom, Almosnino and Zorea [18] , [17] for obtaining

the aerodynamic characteristics of complex configurations at high angles of attack to slender bodies with or without low aspect ratio wings.

Some experimental work carried out by Rom, Sharir and Portnoy [45] studying the effects of jets injection on the reduction of side forces acting on a slender body at angles of attack is presented as indication to methods of control of the aerodynamic effects at these flight conditions.

2. CALCULATION OF THE AERODYNAMIC CHARACTERISTICS OF SLENDER WINGS AND BODIES AT HIGH ANGLES OF ATTACK.

There are a number of methods for the calculation of aerodynamic characteristics of wings and bodies, presented by Maskew [1,2], Margason and Lamar [3], Woodward [4], as well as by the Boeing method [5,6]. However, those methods are limited in their solutions. For example, Maskew's method [1,2] includes the effect of the rolling up of the wake, but is unable to model the leading edge vortices and the non linear lift generated due to their effects. The model of the body in that method is unable to represent the vortices shed from the nose or from other parts of the body which cause non linear effects. Margason and Lamar [3] or Woodward's program [4] do not take into account the rolling up of the wake, and therefore cannot evaluate the aerodynamic characteristics at high angles of attack, for low aspect ratio wings with side edge or leading edge vortex separation. The first program [3] represents the body in a too simplified manner, taking instead only its projection on a horizontal plane, while the latter [4] represents the body by source panels, which are a fair representation for thickness, but are unable to model vortex separation, thus failing at moderate and high angles of attack. Modification of the last two methods try to evaluate the nonlinear lift by superimposing Polhamus [7] and modified Polhamus [8] methods on the linear results. However, in these cases the results are not always accurate and do not model the flow field, the local effects, the correct load distribution or effects of close interactions.

The method developed by the Rubbert [5,6] et al. using a doublet lattice (which is equivalent to the vortex lattice) resulted in a much refined program, and its results are accuracte in many cases. The

method takes into account the rolling up of the wake and its effect on the wing. However, the use of Smith's [9] model of conical flow to describe the initial form of the leading edge vortices results in an incomplete model which cannot deal with secondary separations, and which seems too complicated for the description of close interaction between the vortex flow field and wakes of a closely coupled canard-wing configuration. The description of the body in this method lacks the possibility of representing body shedding of vortices. The problems discussed here are also typical to other methods which try to solve complex configurations of general form [10, 11, 12, 19, 20, 21, 22, 23, 24].

In the NASA Workshop (Ref. 1), the papers dealing with configurations which include bodies use the ideal of "Annular Wing" formed by a vortex lattice, (as for example appearing in the works of Thomas, Miranda, Palko, Heltsley in Ref. 1). However, none of these works deal with the rolling up of the wake, nor with shedding vortices from the body.

The shedding of a pair of vortices from slender bodies may occur already at quite small angles of attack. The pair of vortices remain symmetrical up to about 25-35 degrees, and then occurs a phenomenon of asymmetry in the flow.

Description of the phenomena of body vortices may be found for example in the works of Mendehall and Nielsen [25], Clark and Nelson [26], Angellucci [19], [20] and Smith [46]. A review of the method trying to describe bodies with vortex shedding appears in a paper by Nielsen [27]. Further investigations of this problem are discussed by Angelucci [19], [20], Fiddler [28], and Marshall and Deffenbough [29].

Most of these works use semi-empirical data for calculations.

2.1. The Non-linear Modified Vortex Lattice Method Calculation of Longitudinal Aerodynamic Coefficients of Slender Wings at High Angles of Attack

Rom and Zorea [13,14, 15, 16] introduced a modified vortex lattice method, handling the wing and its wake as one system, enabling the shedding of vortices not only from the trailing edge or the side-edge, but also from the leading edge or from within the wing surface. The vortices which were divided into a number of finite segments, were allowed to roll up and form the structure of the three dimensional wake. Very accurate results were obtained for various rectangular, triangular and swept-back low aspect ratio wings, including their non linear characteristics. Special care was taken for the treatment of the singular vortex element to avoid numerical problems, and to represent closely the actual phenomenon.

This research program which was supported in part by AFOSR Grant No. 71-2145 has been expanded to include the body effects. Some results of this new effort is being supported by DAERO Grant No. 78-G-021. This further development is presented by Rom, Zorea and Almosnino [17,18], where a general method for calculation of the aerodynamic characteristics of wings and multiple lifting surfaces in subsonic flow at high angles of attack was developed. The new method can handle complex planforms such as closely coupled canard-wing-tail combinations, various flaps, elevators, winglets, dihedral angles as well as ground effects. This presentation of the analysis is based on the results presented in References 17 and 18.

2.1.1. Basic Concepts

The lifting surfaces of the configuration, (such as wing, canard, horizontal tail, etc.),are divided into sub-surfaces (Fig. 1). Each subsurface is then divided into trapezoidal or triangular cells. A bound "horse-shoe" vortex is placed in each cell, as described in Fig. 1. In order to satisfy the boundary condition for the flow to be parallel to the surface of the wing, a control point is placed in each cell, (Fig. 1). The shedding of the free vortices (which represent the wake) is presented as an option for the user, who has a large variety of possibilities available (for example: from trailing edge, side edges, leading edge). Each free vortex is divided into a number of finite segments, and a half-infinite last segment. The Biot-Savart law enables the calculation of the velocity induced by a vortex segment $\overline{AB}$ of strength K on a point C in the flow field:

$$V_c = \frac{K \cdot (\cos \widehat{BAC} + \cos \widehat{CBA})}{4\pi r} \qquad (1)$$

(The last equation is in scalar form, and "r" is the distance between the point C and the segment $\overline{AB}$).

The iterative procedure starts with the calculation of a geometric influence matrix, with the free vortices being straight lines shed at an angle to the surface, as an initial condition.

The boundary condition at the control points enables the construction of a set of linear equations. A typical form:

$$
\begin{bmatrix}
H_{11} & H_{12} & H_{13} \\
(n\times n) & (n\times m) & (n\times k) \\
H_{21} & H_{22} & H_{23} \\
(m\times n) & (m\times m) & (m\times k) \\
H_{31} & H_{32} & H_{33} \\
(k\times n) & (k\times m) & (k\times k)
\end{bmatrix}
\cdot
\begin{bmatrix}
K_1^1 \\ \vdots \\ K_n^1 \\ K_1^2 \\ \vdots \\ K_m^2 \\ K_1^3 \\ \vdots \\ K_k^3
\end{bmatrix}
=
\begin{bmatrix}
\hat{w}_1^1 \\ \vdots \\ \hat{w}_n^1 \\ \hat{w}_1^2 \\ \vdots \\ \hat{w}_m^2 \\ \hat{w}_1^3 \\ \vdots \\ \hat{w}_k^3
\end{bmatrix}
\qquad (2)
$$

Each sub-matrix H_{ij} represents the influence of subsurface i on subsurface j. (In the example above there are three subsurfaces). The order of each submatrix is written in parenthesis, and n, m, k defines the number of cells in each of the subsurfaces 1, 2,3, accordingly. The strength of the bound vortex in cell number j, of subsurface i is denoted by K_j^i, while $\hat{w}_j^i$ is the component of the free stream velocity normal to the surface of the wing, at the control point of cell number j, of subsurface i. Column vector K_j^i is to be solved. When the program is solved for the strength of the bound vortices, it also calculates the aerodynamic coefficients, checking for their convergence (except for the first cycle).

The aerodynamic coefficients are C_L, C_{D_i}, C_M. The program also calculates the center of pressure X_{cp}, according to the following formulae:

The lift coefficient (including all possible terms):

$$C_L = \frac{2}{S_{Ref}} \int_o^{b/2} C_j C\ell \, dy = \frac{4}{US_{Ref}} \sum_{j=1}^{N_s} \{ \sum_{j=1}^{N_c} [(1 + \frac{u}{U} - \frac{v}{U}\frac{\Delta x}{\Delta y}) \cdot K]_{ij} \Delta y_j \} +$$

$$+ \frac{-4}{US_{Ref.}} \sum_i \sum_j (\frac{v}{u} \cdot \Delta K \cdot \Delta x)_{ij} \qquad (3)$$

Here ΔX_{ij}, Δy_{ij}, Δz_{ij} are the cartezian components of a bound vortex segment ij in the direction of x, y, z accordingly, while u_{ij}, v_{ij}, w_{ij} are the disturbance velocities calculated in the middle point of each vortex segment belong to the wing surface. The second term on the right hand side of Eq. (3) is of second order, and it expresses in general form the part of the in-surface trailing vortices to the lift, being usually ignored.

The induced drag coefficient and the pitching moment coefficient are given in Eq. (4) and (5):

$$C_{D_i} = \frac{2}{S_{Ref.}} \int_o^{1/2} C_l C\ell_l (tg\alpha_{ind.})_j \, dy =$$

$$= \frac{-4}{US_{Ref.}} \sum_{j=1}^{N_s} \sum_{i=1}^{N_c} [(\frac{w}{U} \Delta y + \frac{v}{U} \Delta z) \cdot K]_{ij} \qquad (4)$$

$$C_M = \frac{4}{US_{Ref.}} \sum_{j=1}^{N_s} \{ \sum_{i=1}^{N_c} [(1 + \frac{u}{U} + \frac{v}{U}\frac{\Delta x}{\Delta y}) \cdot K]_{ij} \Delta y_j \cdot$$

$$\cdot \frac{(X_{ij} - X_{Ref.})}{C_{Ref.}} \} + \frac{-4}{US_{Ref.}} \sum_{j=1}^{N_s} \{ \sum_{i=1}^{N_c} [(\frac{w}{U}\Delta y + \frac{v}{U}\Delta z) \cdot K]_{ij}$$

$$\cdot \frac{(Z_{ij} - Z_{Ref.})}{C_{Ref.}} \} \qquad (5)$$

$X_{Ref.}$, $Z_{Ref.}$ are x and z coordinates of pitching moment reference point. The second term on the right-hand side of Eq. (5) expresses the rolling moment because of induced drag, and it is not negligible in the calculations of complex configurations, such as canard-wing at high angles of attack.

The center of pressure is given by definition:

$$X_{c.p.} = \frac{-C_{Ref.} \cdot C_M}{C_L} \qquad (6)$$

(measured from $X_{Ref.}$)

In general, it should be noted that some of the assumptions made when neglecting terms like those containing the effect of sidewash, proved to be incorrect in strong interactions between canard wake and wing surface, and in the case of strong leading edge vortices. Thus the calculation of aerodynamic coefficients in general cases should include all possible contributing factors.

The program uses an iterative process for the re-calculation of the trajectories of the free vortices, until convergence of aerodynamic coefficients is achieved. (The strength of those is calculated after the solution for the strength of the bound vortices).

The procedure is as follows:

Each point (i) of a segment of a free vortex is moved according to Euler's method of integration

$$y_i^{(2)} = y_{i-1}^{(2)} + \frac{v_i^{(1)}}{U + u_i^{(1)}} \Delta X \qquad (7)$$

$$z_i^{(2)} = z_{i-1}^{(2)} + \frac{w_i^{(1)}}{U + u_i^{(1)}} \Delta X \qquad (8)$$

Here $u_i^{(1)}$, $v_i^{(1)}$, $w_i^{(1)}$ are the Cartesian components of the induced velocity on point (i), before moving it. $y_i^{(2)}$, $z_i^{(2)}$ are the new y and z coordinates of point (i). (The flow is considered steady).

More sophisticated integration methods should be applied in cases where strong disturbances are expected, such as in the cases of very close interactions between lifting surfaces, or very low aspect ratios. The integration process continues iteratively until convergence of all free vortices is achieved, or until the process exceeds a prefixed number of iterations. The influence matrix is reclaculated, leading to a new strength of each bound vortex. Aerodynamic coefficients are then recalculated, and all the process starts again until convergence of the coefficients is achieved (see flowchart of the method, Fig. 23).

The effect of compressibility is taken into account by applying Goethert rule and incorporating it into the computer program.

The accuracy of this rule and its application to the vortex flow over wings has been discussed also by Rubbert and Brune [30].

By using this compressibility correction, the present method can now be used over the range of subsonic Mach numbers up to the critical Mach number.

2.1.2. Results of Calculations

(a) Computational Aspects

The use of the singular vortex element in vortex lattice methods presents some difficulties. The main one is the too high velocities induced by the vortex on points which are too close to the vortex segment.

The reason for that is the fact that a potential singular vortex does not exist, due to viscous effects. Some attempts were made to overcome this problem, for example Rom and Zorea's [13] attempt to use the model of Spreiter and Sacks [31] for the calculation of the radius of each vortex core, or Maskew's "Sub Vortex Techniques" [1],[36]. One of the main conclusions from these attempts was that it is satisfactory in most cases to use a general "cut off distance" for all the vortices in the model. The last method saves a lot of computing time, and it was used in the present method. The results show that it is reasonable to use a "cut off distance" similar to the width of the partition into elemental panels. Strong vortices such as those shed from a leading edge may require a larger "cut off distance".

Another problem arises when shedding too many free vortices. Because of the singularity of each potential vortex, the convergence of the free vortices trajectories is either very slow or completely impossible. The multiplicity of free vortices is a result of a dense partition into elemental panels, (which is favorable when the aim is to achieve a smoother load distribution). The present method overcomes this difficulty by giving the option to merge close free vortices into one vortex, of a strength which is the sum of the strength of the merged vortices. The number of free vortices is thus reduced, while the number of elemental panels remains as it was.

Results of the present method show that merging too close free vortices is especially effective in the cases of leading edge separation, in wings of low aspect ratio (AR < 2) with sharp leading edges. In

these cases the convergence was much more rapid and the nonlinear aerodynamic coefficients calculated showed very good agreement with experimental results. When no merging was applied, the calculated results showed weaker nonlinear behavior than expected, resemling experimental results for wing with round leading edges, (see for example Ref. 35). The effect of merging free vortice on aerodynamic coefficients is strong when dealing with vortices which pass upon the wing surface; otherwise the effect is negligible.

b) Comparison with Experimental Results

1. Closely Coupled Canard and Wing, with Leading Edge Separation

The configuration was chosen for comparison with Ref. (32) and it is shown in Fig. 2. Both the canard and the main wing are of aspect-ratio 1.66, and of similar form. Two vertical positions of the canard were checked, as it is shown in Fig. 2. The canards are vertically located at $z/\bar{C}_c = 0.2, (-0.29)$ above (beneath) the main wing plane accordingly, and their aft point is located longitudinally at $0.1\bar{C}_c$ from the main wing vertex. (Here $\bar{C}_c$ is the canard mean geometric chord). Behrbohm [32] states that the model used for experiments had round leading edges, which considerably reduce the nonlinear effects. Indeed, when using the present method with the option of merging free vortices, (the effect of which was described before in part (a) of this Chapter), the calculated results for the lift coefficient of the high canard were higher than the experimental ones (Fig. 3a, upper curve).

By assuming separation of vortices without merging to be a better approximation of the actual separation from the rounded edges, the calculated results obtained were better than those previously described,

although somewhat lower than the experimental ones (Fig. 3a). The first results however, may be an indication for the maximum nonlinear effect that can be obtained, should the leading edges be sharp.

It should be noted that the present method also gives the correct tendencies for the low canard, in comparison with the high canard. The interesting behavior of the low canard can be observed in Fig. 3b, where the lift coefficient increases linearly up to an angle of attack of approximately 15^{o}, and then a strong non-linear effect occurs, up to 20^{o}.

This phenomenon has been observed both in the experimental and the calculated results. It is explained by the fact that the free vortices of the canard stay below the main wing surface up to a certain point, and as the angle of attack increases above the point, the free vortices shed from the canard pass above the main wing surface, causing positive interference and as a result non-linear lift is obtained. The low canard lift coefficient even equals the high canard lift coefficient at an angle of attack of 20^{o}.

Correct tendencies for the high and low canards can be observed also from Fig. 4 where the change in the pitching moment coefficients is described (versus the lift coefficient).

The effect of interaction between high canard leading edge vortices and wing leading edge vortices can be seen from Fig. 5. Noteworthy too is the fact that due to the upwash effect of the wing on the canard, the leading edge vortices of the canard leave its surface at an angle higher than half of the angle of attack. In general, this accepted initial value which was fair enough for single wings, may lead to numerical problems in some of the strong interaction problems such as the case of a low canard.

In the latter case numerical problems arise because of unfitting initial conditions, when the wake of the canard tries to cut through the wing surface. The low canard case also shows tendencies of instability in the flow, within a limited range of angles of attack. However, the high canard case which is much more common does not present any problems. An example of the load distribution is presented in Fig. 6.

2. Canard and Wing Interference with no Leading Edge Separation

The configurations chosen were three variations of a basic model experimented by Gloss [33]. The basic form of the configuration is shown in Fig. 7. The model consists of a trapezoidal main wing of AR = 2.5 and a swept back canard of AR = 4.12. The first variation (denoted as configuration No. 2) consists of a 51.7 deg. swept back canard, which has 0 deg. dihedral angle. The second variation (denoted as configuration No. 3) consists of a 51.7 deg. swept back canard which has 18.6 deg. dihedral angle. The third variation (denoted as configuration No. 4) consists of a 60 deg. swept back canard which has 0 deg. dihedral angle.

All canards' roots were located at a height of $z/\bar{C} = 0.185$ above the wing plane, ($\bar{C}$ is the wing mean geometric chord), and at a longitudinal distance of $x/\bar{C} = 1.304$ from the model nose to the canard leading edge. The partition chosen for the calculations was NC = 4, NS = 10 (using trapezoidal cells) both for the canard and for the main wing, in all cases.

Free vortices were shed from the trailing edges and from the side edges. All three cases showed very good agreement between the experimental and the calculated results as can be seen from Figs. 8 to 12. The calculated results depart from the experimental results only when stall effects

start. Trying a denser partition of NC = 4, NS = 10 for the canard, with NC = 10, NS = 20 for the main wing had very little effect on the results, apart from the higher computer time needed for the solution.

An interesting comparison is shown in Fig. 13 and 14. The present method is compared to calculated results of modified Polhamus methods (from Ref. 33). It can be seen clearly that the present results for the lift coefficient are in better comparison with the experimental results, in addition to evaluation of the load distribution and the strength and form of the wake, which are not calculated by the modified Polhamus methods.

3. Secondary Vortex Formation

As an example of this phenomenon a view of main and secondary leading edge vortices was sketched for a delta wing of AR = 2, at 20 deg. angle of attack (Fig. 15). The calculated relative strength of those vortices appear in a Table (Fig. 15). (Trailing edge vortices were omitted from Fig. 15 in order to get a clearer view). In delta wings of AR < 2, the appearance of the secondary vortex is found to be at an inner region than the example given as indicated by experiments.

4. The F-4-E Planform in Compressible Flow

In the following example application of the method has been made to analyse a complex planform also making use of the Goethert rule for the evaluation of the compressibility effects.

The geometry of the model includes the main wing which has a dihedral of 12 deg. on its outer span and a "saw tooth" form on its leading edge. The tail planform has a negative angle fo dihedral (-23.25 deg.) and is operating as a mono-block control. Both the main wing and the tail are

extended to the center line. A schematic description of the geometry of the model partitioned into elemental panels is shown in Fig. 16. The calculated results are compared with the experimental results of Ref. 34. Very accurate results are obtained for the lift coefficient variation with the angle of attack, at M = 0.6 and also at M = 0.8, up to the stall conditions, (Fig. 17).

Good results are also obtained for tail deflections up to -16 deg. There was no point in comparing results for the pitching moment, because of the difficulty to correct the calculations for the presence of the complex body; however, deflections of the tail show the right tendencies in the calculated pitching moment.

The experimental results for induced drag coefficient fall between the calculated results for the case of full leading-edge suction drag and those calculated for zero leading-edge suction drag.

c) Cruciform Configuration in Subsonic Flow

The non-linear characteristics of a cruciform combination of rectangular wings are evaluated by the present method (at 0.0 Mach number). The configuration is combined of cruciformed rectangular main wings and tails, described in Fig. 19. The calculated lift and pitching moment coefficients show a strong non-linear variation with increasing angle of attack (Fig. 20). The existence of the "turning point" in the curves of C_L, C_M, C_{D_i} (Fig. 20) is explained by examining the path of the free vortices shed by the wing. At about 12^o those vortices pass very near and below the upper tail, causing a considerable loss of lift on that part. Further increase of the

angle of attack would cause those free vortices to make their way above tail, gaining lift again. It should be noted that there is some loss of stability in the region of the turning point, as seen from the pitching moment curve slope. Experimental data on cruciformed wings configurations indicate similar variation. Results are sensitive to the relative location and shape of the tail.

d) Computer Time

Computing time for a complex configuration is at present rather high (about 2000 sec on IBM 370/168 type). However, computation time may be considerably reduced, should the program be optimized. The use of the iterative scheme is time saving in itself.

2.2. A Method for Calculations of the Aerodynamic Characteristics of Slender Bodies with Vortex Separation

The use of vortex elements enables the proposition of a simple model for representing the separation of vortices from the body surface.

Mainly the model of the body is that of an "Annular Wing", built of a vortex lattice (see for example Ref. 2,23), with the possibility to separate vortices from the surface. The separation point in the model is located in the junction between two adjacent bound vortices or in some point located on the line of the trailing in-surface vorticity. The vortex arrangement on a cylindrical body is shown in Fig. 21, together with an example for the method of separation between two adjacent elemental panels.

This method of separation enables also to separate vortices from pre-chosen regions of the body surface, according to the separation theory to be chosen.

References 27, 28, 29, 46, for example, discuss the problem of determining a criterion for the separation of vortices from the surface of slender bodies at high angles of attack. However a thorough survey of the proposed criteria for separation is under consideration, aimed to choose a general model which should be also as simple as possible for the purpose of incorporation with the method of calculation. Ref. 29 for example, presents an interesting method for calculating aerodynamic characteristics of bodies having vortex separation at high angles of attack, but the cost in C.P.U. time for utilizing this method seems to make it unattractive for incorporation with a general method for complex configurations.

Other potential elements such as point sources or sinks might be needed for the description of a blunt nose of a body for example.

Those elements are distributed inside the body as described in Fig. 21.

It should be noted that the calculation of wing-body configuration is carried out essentially in the same way as described for the case of wings (Chapter 2.1.1. in this report) with the geometrical influence coefficients of the body taking proper places in the general matrix (Eq. 2).

A general flow chart for the procedure of calculation appears in Fig. 23.

A method for the representation of thick wings appears in Fig. 22. Here too potential elements such as line sources/sinks might be needed for a complete description of thickness and of round edges, (apart from the vortex element).

For more accurate calculation of the local pressure coefficient, methods such as the "Sub-Vortex Technique" by Maskew [1],[36] may be used, after adaption to the three dimensional case.

3. EXPERIMENTAL STUDY OF THE AERODYNAMIC CHARACTERISTICS OF SLENDER BODIES AND THE EFFECT OF INJECTED JETS, AT HIGH ANGLES OF ATTACK.

3.1. Lateral Forces and Moments Acting on a Body at High Angles of Attack at Subsonic and Transonic Speeds

The occurrence of asymmetric vortex flow and hence side forces and yawing moments on bodies of revolution at high angles-of-attack and zero sideslip has been observed experimentally and is under intensive studies at various laboratories.

All previous investigations have shown that the nose shape is one of the most significant parameters affecting side force characteristics. It has been found experimentally that it is possible to reduce side forces by the use of devices causing boundary layer transition or vortex generators on the nose.

In the present investigation air jets blown from a body of revolution are used in order to reduce the side forces.

There are many parameters that may affect these side forces such as the position of the stations on the body for these jets, the polar angle of each station, the mass flow and velocities of the jets. Some of these parameters have been investigated and reported in this paper.

At moderate angles of attack the adverse cross-flow pressure gradient on the leeside of the body causes the boundary layer to separate and then to roll-up into a system of distinct vortices.

The rolled-up vortex sheet may stay joined to the body and be continuously fed from the separated boundary layer or it may leave the body entirely further downstream. Since the boundary layer separation is caused by the adverse pressure gradient, the separation line may be

expected to be close to the line of the minimum pressure coefficient on the leeward side of the body [37].

Due to geometrical irregularities of the nose of the body or irregularities in the flow direction one side of the boundary layer may separate first from the body, retaining a certain vortex strength in the corresponding rolled-up vortex sheet. The other side of the boundary layer may remain attached and separate only further downstream on the body with a correspondingly stronger vortex. Thus we find an asymmetric vortex system generated behind the body at high angles of attack. This is supported by the results of Ref. 38 where it is shown that the side forces are connected to asymmetry of circumferential pressure distribution and asymmetry of vortex sheet separation on the leeside of the body. In the visualization tests of Ref. 37 it is shown that as the angle of incidence increases the separation line is shifted towards the windward side. The circumferential angles of separation (ϕ_{s1}, ϕ_{s2}) as measured from the windward meridian, indicated a non-symmetrical separation on the cylindrical afterbody when laminar boundary layer conditions exist. This asymmetry increased with increasing angle of attack. The maximum angular difference very nearly coincided with the maximum measured side force. (The maximum angular difference was of the order of 20° to 40° for the sharp and slightly blunted slender noses respectively, while this difference decreased to 5° to 10° for the lowest fineness ratio nose).

At high angles of attack the side vortices could grow and separate at several points along the body: this phenomenon was found by [37], [38] and [39].

The phenomenon of these lateral forces can be also modeled by the umpulsively started cross-flow analogy. The calculation of side forces and pressure distributions on inclined cylindrical bodies at high angles of attack is presented by Lamont and Hunt in Ref. 40 and 41. Using the cross-flow analogy the induced lateral flow field is evaluted without specific reference to the state of the boundary layer on the body. The validity of this assumption must be studied.

The generally accepted results of the investigations of the phenomena associated with vortex asymmetry on slender bodies at high angles of attack are the following:

(1) The initial direction of the side force is unpredictable because of its connection with small irregularities in the nose geometry; however once the direction is established this does not change as the incidence angle is increased.

(2) Reynolds number has no effect on the angle of onset of asymmetry but does have an effect on the magnitude of the side force. (The Reynolds number effect is in defining the boundary layer in the sense of whether it is supercritical or subcritical. For instance in Ref. 40 the relation of $C_{Y_{max}}$ in the supercritical to the subcritical is 1.5/2.5).

(3) The magnitude of the side forces increases with increasing the finess ratio of the nose.

(4) Side forces remain small below $\alpha = 25^{\circ}$. Beyond this they increase and reach peaks at around $35^{\circ} - 40^{\circ}$, depending on the Mach number and geometrical configuration.

(5) The magnitude of the side force is decreased by as much as 80% when a boundary layer strip is installed on the windward side. This is a result of early transition to turbulent boundary layer.

Side forces and moments may be potentially hazardous to the control and stability of slender configurations such as fighters and modern missiles, at high angles of attack. These side forces and moments may be overcome by sufficient control authority and autopilot gain margin so that flight control is maintained, or by aerodynamic devices to suppress the asymmetric vortex pattern.

In Refs. [42,43 and 44] the investigators have pointed out that the nose shape is a most significant parameter affecting side forces, therefore adding transition strips or vortex generators on the nose can reduce the side forces.

These devices cause regular symmetric boundary layer flow on the nose of the body, thus eliminating the previously discussed asymmetric boundary-layer separation and so the associated vortex system is symmetric, therefore, eliminating the large side forces and moments.

In the work of Keener and Chapman [42] reduction of side forces is achieved by adding meridianal strips of grit at the angular position $\theta = \pm 30^{\circ}$. In Ref. [43], the positioning of a ring on the nose caused a great reduction in the large yawing moments at high angles of attack. In the work of Clark, Peoples and Briggs [44] the additon of vortex generators at the nose was sufficient to cause the separated vortices to be more symmetric at the critical angles of incidence. In this present investigation air jets blown from the body of revolution are used to affect flow symmetry and reduce the side forces and moments.

This is shown by an experimental investigation wherein the side forces and moments are measured with the air jets blown at different blowing coefficients, C_μ.

Preliminary tests have been carried out in the high subsonic and the transonic flow regions.

3.2. The Effects of Jets Injected Near the Nose of the Body on the Lateral Forces and Moments at High Angles of Attack, in Subsonic and Transonic Speeds.

3.2.1. The Model and Facilities for the Experiments

The experiments described herein were conducted in the Subsonic Wind Tunnel of the Aeronautical Research Center of the Technion with a cross section of 1m x 1m.

The model shown in Fig. 24 is an axisymmetric body of revolution with a body diameter of 3 in. and an overall finess ratio of 6.

Three different forebodies could be used: a pointed cone, a blunt cone and a blunt ogive (shown in Fig. 24).

After conducting some preliminary tests it was decided to blow jets from two sections, one very close to the nose apex and the second further along the nose (Fig. 24). At each station three pairs of holes were drilled at $\pm 60^\circ$ and $\pm 30^\circ$ as indicated in Fig. 24 and the diameter of the injection holes was 1.2 mm perpendicular to the body's axis (this diameter was chosen so as to obtain blowing velocities of the same order of magnitude as the tunnel flow speed).

A system of rigid and flexible tubing was arranged in the model so as to obtain symmetrical blowing of the jets through a different pair of holes each time.

Throughout the experimental program, a six component internal strain gage balance was used to measure the aerodynamic forces and moments. This balance was very sensitive to side forces.

The experimental system is capable of changing the rate of flow and of providing measurements of the pressures and of the rates of flow.

The experiments were conduced at a flow speed of 20m/sec (for a Reynolds number of 1.08×10^5 based on the diameter) with the pointed cone configuration and for a range of angles of attack of $30^\circ - 56^\circ$. In the preliminary tests we found this configuration to give the highest values of side force.

Tests with no injection and a few tests with injection were repeated in order to verify the repeatability of the test results. The jets were also blown without flow and the measured side force was found to be negligible, showing that the blowing is symmetrical.

Qualitative tests for flow visualization were also performed. Using oil paints on the model, the development of the stream lines on the body was followed. The flow patterns indicated positions of separation as shown in Fig. 25.

3.2.2. Results

The results of the tests can be summarized according to the angular position of the jets on the model:

Blowing at 60°- At both stations increased values of the side force coefficients in comparison to those obtained without blowing were observed.

Blowing at $+ 30^\circ$ - At station II, high values of side force coefficients were observed with increasing rate of flow. At station I, two interesting results were observed (see Fig. 26) - the line of $C_\mu = 166.33 \times 10^{-5}$,

where the jets kept the side force coefficient from growing until 40° and then caused a peak higher than the original; and the experiments for $C_\mu = 289.34 \times 10^{-5}$, in which the side force coefficient followed the original line to an angle of 40° where there was a change of sign until a negative peak was reached at 44°, followed by a rise to a peak similar to the original.

Blowing at 30° - At station II, a reduction of the maximum side force coefficient up to 50° was observed in the two experiments shown in Fig. 27.

Both the curves $C_\mu = 33.25 \times 10^{-5}$ and 285.7×10^{-5} decrease from their maxima at $\alpha = 46°$ to zero side force coefficient at $\alpha = 53°$.

The yawing moment coefficient was decreased in these experiments by up to 30%.

At station I, a meaningful reduction of side force for certain angles of attack was observed (Fig. 28).

On the yawing moment coeffcient curve (Fig. 29) we observed a meaningful reduction with jets blowing compared to the original curve.

On examination of the side force coefficient versus the rate of flow diagram (Fig. 30) it is obvious that there is an optimum rate of flow for blowing the jets. The arrows on the Figure point to a concentration of many test results (on this curve the side force direction is opposite to its direction on Fig. 31).

Side Forces Versus Reynolds Number

The experiments of this investigation were conducted in a range of Reynolds number from 1.07×10^5 to 1.69×10^5, based on the body's diameter.

Fig. 31 shows the change of side force coefficient versus crossflow Reynolds number, at $C_\mu = 21.6 \times 10^{-5}$.

Consistency of Results

Fig. 32, which describes the experiments without blowing shows good consistency up to 48°. From this point scattering of results can be observed but they are still acceptable as consistent (the scattering of results is a characteristic phenomenon in all works on this subject. It is common practice to attribute this to the fact that the side forces are sensitive to changes in the nose alignment and in the experimental conditions and also to mounting induced vibrations.

In the blowing experiments which were repeated, similar amplitudes were observed but the sign of the side force changed in some cases.

From the experiment that was conducted without flow it was found that no side forces were measured by the balance and the conclusion is that the blowing during the experiments was symmetrical.

Analysis of Oil Flow Photographs

From a comparison of the pictures with no blowing to those with blowing which was carried out for two angles of attack, $\alpha = 46^\circ$ and $\alpha = 48^\circ$ (on which the maximum no blowing side force coefficient was observed), the following conclusions can be derived:

(1) The blowing of the jets delays the separation point to much further downstream on the body (because of the transition to turbulent flow).

(2) The flow separation lines on each side become more symmetrical. These results are similar to the results described in Refs.40,41 and 42, in which the investigators added rigid elements on the nose.

Preliminary Tests in the High Subsonic and in the Transonic Regions

The tests were carried out in the transonic wind tunnel of the Aeronautical Research Center of the Technion, which has a cross section of 60cm x 80cm. The model is the pointed cone nose (Fig. 24). The investigations included experiments with and without jet injection at Mach numbers of 0.6 and 0.8, for angles of attack between 35° to 56°. The injection took place at station A (Fig. 24), at an angle of -30° and with a blowing coefficient of $C_{\mu} = 149.4 \times 10^{-7}$ for $M = 0.6$ and $C_{\mu} = 84.07 \times 10^{-7}$ for $M = 0.8$.

Schlieren photographs were taken during the tests. At $M = 0.6$ the blowing had only little effect on the reduction of the side force coefficient (Fig. 33), although it reduced to some extent the yawing moment (Fig. 34). However, at $M = 0.8$ both side force and yawing moment were considerably reduced within the range of the angles of attack $35^{\circ} < \alpha < 48^{\circ}$ (Figs. 35, 36). The effectiveness of the blowing disappeared for angles of attack higher than 48°.

From Shlieren photographs(Fig. 37) it can be seen that a shock wave appeared near the shoulder of the body at $M = 0.8$. However, the flow picture with jet blowing (Fig. 37b) is different from the flow without blowing (Fig. 37a). The considerable reduction in side force and yawing moment at $M = 0.8$ encourages further investigation for the effect of jet blowing.

Effects of Reynolds number, influence of the rate of blowing and shock wave formation should be investigated at these and higher transonic Mach numbers.

4. DISCUSSION AND CONCLUSIONS

4.1. The Modified Vortex Lattice Method for Calculations of Complex Wing Planforms at High Angles of Attack.

The present method offers an efficient means of analysis and design of complex aerodynamic configurations. The good results obtained for strong interaction cases and for non-linear effects encourage further development and refinement of the method. One aim in future development has been mentioned in Section 2.2. of this report, and that is including the presence of bodies with vortex separation. The presence of a body is influencing especially the pitching moment coefficient of wing-body configurations, and also the form of the wake, the pressure distribution and the total lift coefficient at high angles of attack. Another aim in future development should be inclusion of thickness effects for lifting surfaces.

Although expensive for use in the sense of computer time and memory, a correct description of thick wings with round leading edges might give more correct pressure distribution and might enable a good estimate of the induced drag, and of the leading edge suction force.

Thought should be given also to get "smoother" pressure distributions, although present results show that the total aerodynamic coefficients are in good comparison with experimental results even with the simple "block" distribution used.

It should be concluded that the present method can be used for the calculation of aerodynamic characteristics of complex configurations at high angles of attack and at subsonic speed, with reasonable cost in

computing time due to the simplicity of the basic model used.

Using the present method, the analysis holds up to the effects of stall or vortex break-down.

4.2. The Effects of Jets Injection Near the Nose of a Slender Body on the Side Force and Yawing Moment at High Angles of Attack

From the results of this research it can be seen that it is possible to reduce side forces and even change their sign by blowing symmetric jets from the body as close as possible to the nose apex (the importance is, of course, in reducing the maximum side forces).

The most effective results appear on blowing at an angle of - 30° (on the windward side). It can be seen that the jet blowing is inefficient at angles of attack above 52°.

The amount of blowing used did not cause any change in the normal force drag.

The rate of flow of the jets needed to reduce the side forces is very small. This solution is not sensitive to changes in the rate of flow; increasing the rate of flow did not cause significant changes in side force coefficient.

Effect of Angle of Attack - Increasing angle of attack causes the side force to increase until it reaches a peak at about 50°. Above this angle further increase of angle of attack causes decrease of the side forces.

Angle of Onset Asymmetry - From the results of the experiments it is clear that the blowing jets do not cause any change in the value of the angle of onset of asymmetry.

Jet Control - More effective results in utilizing blowing jets may be achieved by designing a control system which changes the rate of flow as a function of angle of attack.

A control system can be devised to vary the rate of flow in order to keep low values of side force coefficients.

Effect of Reynolds Number and Mach Number Changes

At this stage of tests it is impossible to define the effects of Mach number on side forces.

Further tests are required in order to investigate the effects of both Mach number and Reynolds number on the lateral forces and moments of these slender configurations at high angles of attack with and without blowing.

REFERENCES

1. "Vortex Lattice Utilization,"Workshop held at NASA Langley R.C., NASA SP-405, May 1976.

2. Maskew, B., "Calculation of the three-dimensional potential flow around lifting nonplanar wings and wing-bodies using a surface distribution of quadrilateral vortex rings," Loughborough U. of Tech., Rep. TT 7009, Sept. 1970.

3. Margason, R.J. and Lamar, J.E., "Vortex Lattice FORTRAN program for estimating subsonic aerodynamic characteristics of complex planforms," NASA TN D 6142, 1971.

4. Woodward, F.A., " An improved method for the aerodynamic analysis of wing-body tail configurations in subsonic and supersonic flow," NASA CR-2228 (2 volumes), May 1973.

5. Rubbert, P.E. and Saaris, G.R., "Review and Evaluation of a three-dimensional lifting potential flow analysis method for arbitrary configurations ," AIAA Paper 72-188, Jan. 1972.

6. Weber, J.A., Brune, G.W., Johnson, F.T., Lu, P., and Rubbert, P.E., "A three-dimensional solution of flows over wings with leading edge vortex separation," NASA SP-347, 1975, pp.1013-1032. Also, AIAA Jr. Vol. 14, No. 4, April 1976, pp. 519-525.

7. Polhamus, E.G., "A concept of the vortex lift and sharp edge delta wings based on a leading edge suction analogy," NASA TND-3767, Dec. 1966.

8. Lamar, J.E., "Some recent applications of the suction analogy to vortex lift estimates," NASA SP-347, pp. 985-1011, 1975.

9. Smith, J.H.B., "A theory of the separated flow from the curved leading edge of a slender wing," Tech. Note, Aero 2535, Nov. 1957.

10. Loeve, W., "The calculation of aerodynamic characteristics of wing body combinations at subsonic flight speeds", NLR MP 76017 U, June 1976.

11. Hess, J.L., "Calculation of potential flow about arbitrary three-dimensional lifting bodies," Final Tech. Reprt, MDC J 5679-01, McDonnell Douglas (1972).

12. Uchiyama, N., Mikkilineni, R.P. and Wu, J.M., "The analysis of wing-body combinations at moderate angles of attack," AIAA Paper 78-62, Jan. 1978.

13. Rom, J., Zorea, C., and Gordon, R., "On the calculation of non-linear aerodynamic characteristics and the near vortex wake," ICAS Paper No. 74-27, Aug. 25-30, 1974.

14. Rom, J., Portnoy, H., and Zorea, C., "Investigations of the rolling-up of the vortex wake and calculation of non linear aerodynamic characteristics of wings", *TAE Report No.277*, Technion, Israel Inst. of Tech., June 1976.

15. Zorea, C., and Rom, J., "Vortex Roll-up over and behind wings related to non-linear aerodynamic characteristics", Jr. of Aircraft, Vol. 15, No. 4, April 1978, pp. 193-194.

16. Zorea, C.R., and Rom, J., "The calculation of non-linear aerodynamic characteristics of wings and their wakes in subsonic flow," Collection of Papers - 20th Israel Annual Conf. on Aviation and Astronautics, Feb., 1978, pp. 36-48.

17. Almosnino, D., Zorea, C., and Rom, J., "A method for calculating longitudinal characteristics of wings and multiple lifting surfaces in subsonic flow, and at high angles of attack", Collection of Papers - 20th Israel Annual Conference on Aviation and Astronautics, Feb., 1978, pp. 66-74.

18. Rom, J., Almosnino, D., and Zorea, C., "Calculation of the non-linear aerodynamic coefficients of wings of various shapes and their wakes, including canard configurations," Published in ICAS Collection of Papers of the 11th Congress of ICAS, Lisbon, Sept. 10-16, 1978, Vol. 1, pp. 333-344.

19. Angelucci, S.B., "A multi-vortex method for axisymmetric bodies at angles of attack," Jr. of Aircraft, Vol. 8, No. 12,1971, pp.959-966.

20. Angelucci, S.B., "Multi-vortex model for bodies of arbitrary cross-sectional shapes," AIAA Paper 73-104, 1973.

21. Kandil, O.A., Mook, D.T., and Nayfeh, A.H., "A numerical technique for computing subsonic flow past three-dimensional carad-wing configurations with edge separation," AIAA Paper 71-1, Jan. 1977.

22. Giesing, J.P., "Lifting surface theory for wing-fuselage combination," Rep. DAC 67212, McDonnell Douglas Aircraft Inc., August 1968.

23. Kalman, T.P., Rodden W.P., and J.P. Giesing, "Application of the doublet lattice method to non-planar configurations in subsonic flow," J. Aircraft Vol. 8, No. 6, June 1971.

24. Loeve, W., and Slooff, J.W., "On the use of panel methods for predicting subsonic flow about aerofoils and aircraft configurations," NLR Rep. MP 71018, 1971.

25. Mendenhall, M.R., and Nielsen, J.N., "Effect of symmetrical vortex shedding on the longitudinal aerodynamic characteristics of wing-body-tail combinations," NASA CR 2473, Jan. 1975.

26. Clark, W.C., and Nelson, R.C., "Body vortex formation on missiles at high angles of attack," AIAA Paper No. 76-65, 1976.

27. Nielsen, J.N., "Nonlinearities in missile aerodynamics,"AIAA Paper No. 78-20, Jan. 1978.

28. Fidler, J.E., "Approximate method for estimating wake vortex strength," AIAA Jr. Vol. 12, 5, May 1974.

29. Marshall, F.J., and Deffenbaugh, F.D., "Separated flow over bodies of revolution using an unsteady discrete-vorticity cross wake," NASA CR 2414, June 1974.

30. Brune, G.W., and Rubbert, P.E., "Boundary-value problem of configurations with compressible free vortex flow," AIAA Jr. Vol. 15, No. 10, (Technical Notes), Oct. 1977.

31. Spreiter, J.R., and Sacks, A.H., "The rolling up of the trailing vortex sheet and its effects on the downwash behind the wings," JAS Vol. 18, No. 1, Jan. 1951, pp. 21-32.

32. Behrbohm, H., "Basic low speed aerodynamics of the short coupled canard configuration of small aspect ratio," SAAB TN-60, Sweden, July 1965.

33. Gloss, B.B., "The effect of canard leading-edge sweep and dihedral angle on the longitudinal and lateral aerodynamic characteristics of a close coupled canard-wing configuration." NASA TND-7814, Dec. 1974.

34. Ray, E.J., and Hollingsworth, E.G., "Subsonic Characteristics of a twin jet swept-wing fighter model with maneuvering devices," NASA TN D-6921, Jan. 1973.

35. Kuchemann, D., "A non-linear surface theory for wings of small aspect ratio with edge separation," Royal Aircraft Estab. Rep. AERO 2540, April 1955.

36. Maskew, B., "Subvortex technique for the close approach to a discretized vortex sheet," J. Aircraft, Vol. 14, No. 2, Feb. 1977.

37. Pick, G.S., "Investigation of side forces on ogive cylinder bodies at high angles of attack in the M = 0.5 to 1.1. range," AIAA Paper No. 71-570, 1971.

38. Krouse, J.R., "Induced side forces on slender bodies at angles of attack and Mach numbers of 0.55-0.80,"NSRDC Test. Rpt. May 1971.

39. Thomson, K.D., and Morrison, D.F., "The spacing position and strength of vortices in the wake of slender cylindrical bodies at large incidence," Weapons Research Establishment, Salisbury, South Australia, Tech. Rep. NSA 25, June 1969.

40. Lamont, P.J., and Hunt, B.L., "Pressure and force distribution on a sharp-nosed circular cylinder of large angles of inclination to a uniform subsonic stream,"Jr. of Fluid Mechanics, Vol. 76, pp. 519-559.

41. Lamont, P.J., and Hunt, B.L., "Prediction of aerodynamic out of plane forces on agive-nosed circular cylinders,"Jr. of Spacecraft, Vol. 14, No. 1, Jan. 1977, pp. 31-44.

42. Kenner, E.R., and Chapman, G.T., "Onset aerodynamic side forces at zero sideslip on symmetric forebodies at high angles of attack,"AIAA Paper No. 75-770, 1974.

43. Letko, W., "A low speed experimental study of directional characteristics of sharp-nosed fuselage through a large angle of attack range at zero angle of sideslip," NACA TN 2911, March 1953.

44. Clark, W.H., Peoples, J.R. and Briggs, M.M., Occurrence and inhibition of large yawing moments during high incidence flight of slender missile configurations", AIAA Paper No. 79-968, 1972.

45. Sharir, D., Portnoy, H., and Rom, J., "A study of the effects of jets injected from a slender body of revolution on the side forces acting on it at large angles of attack in low speeds, TAE Report 337, May 1978, Technion,Israel Inst., of Tech.

46. Smith, J.H.B. "Inviscid Fluid Models, Based on Rolled-up Vortex Sheets, for Three-Dimensional Separation at High Reynolds Number", RAE TECH. MEMO AERO 1738, November 1977.

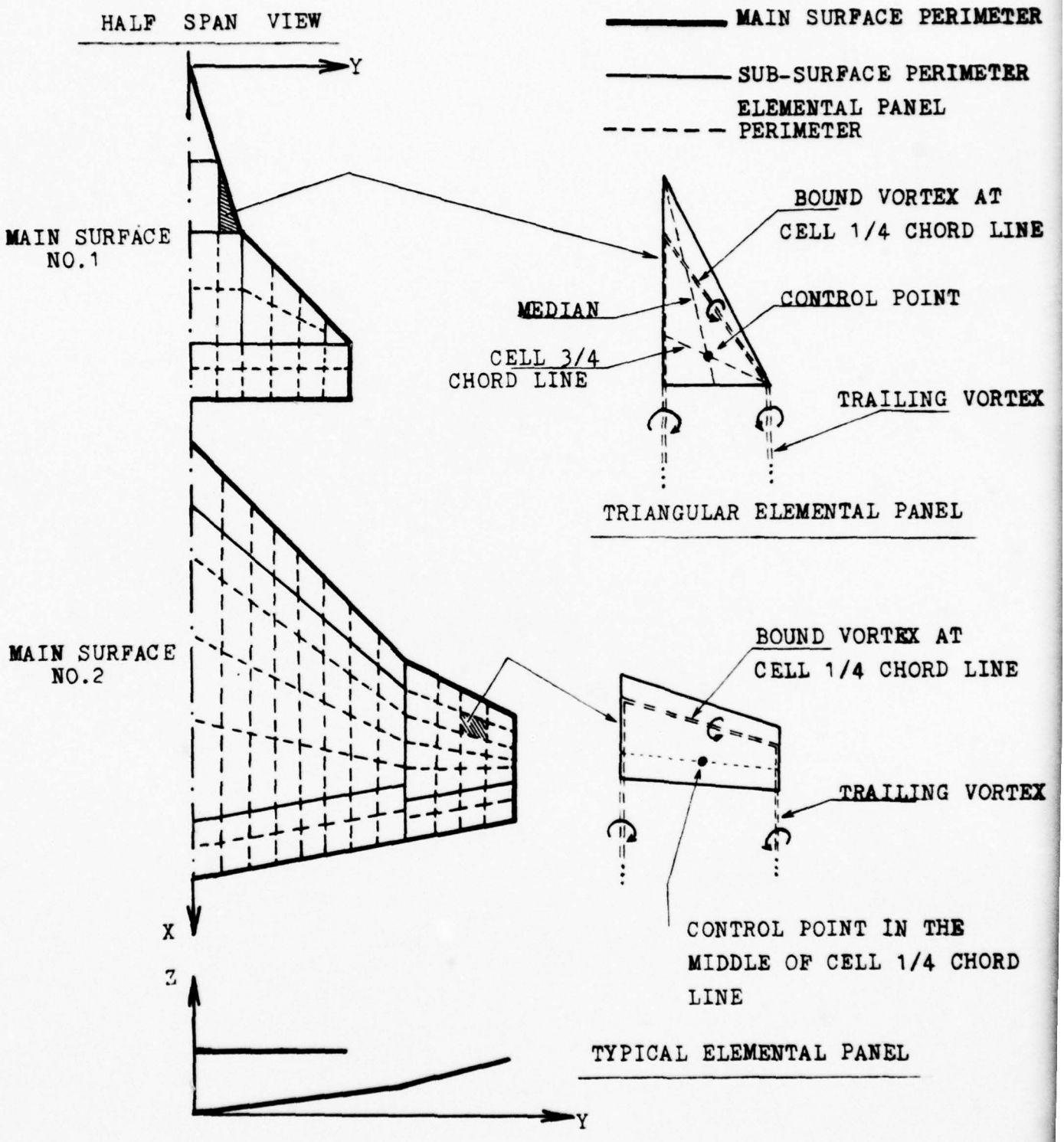

FIGURE 1 - DESCRIPTION OF THE MODEL.

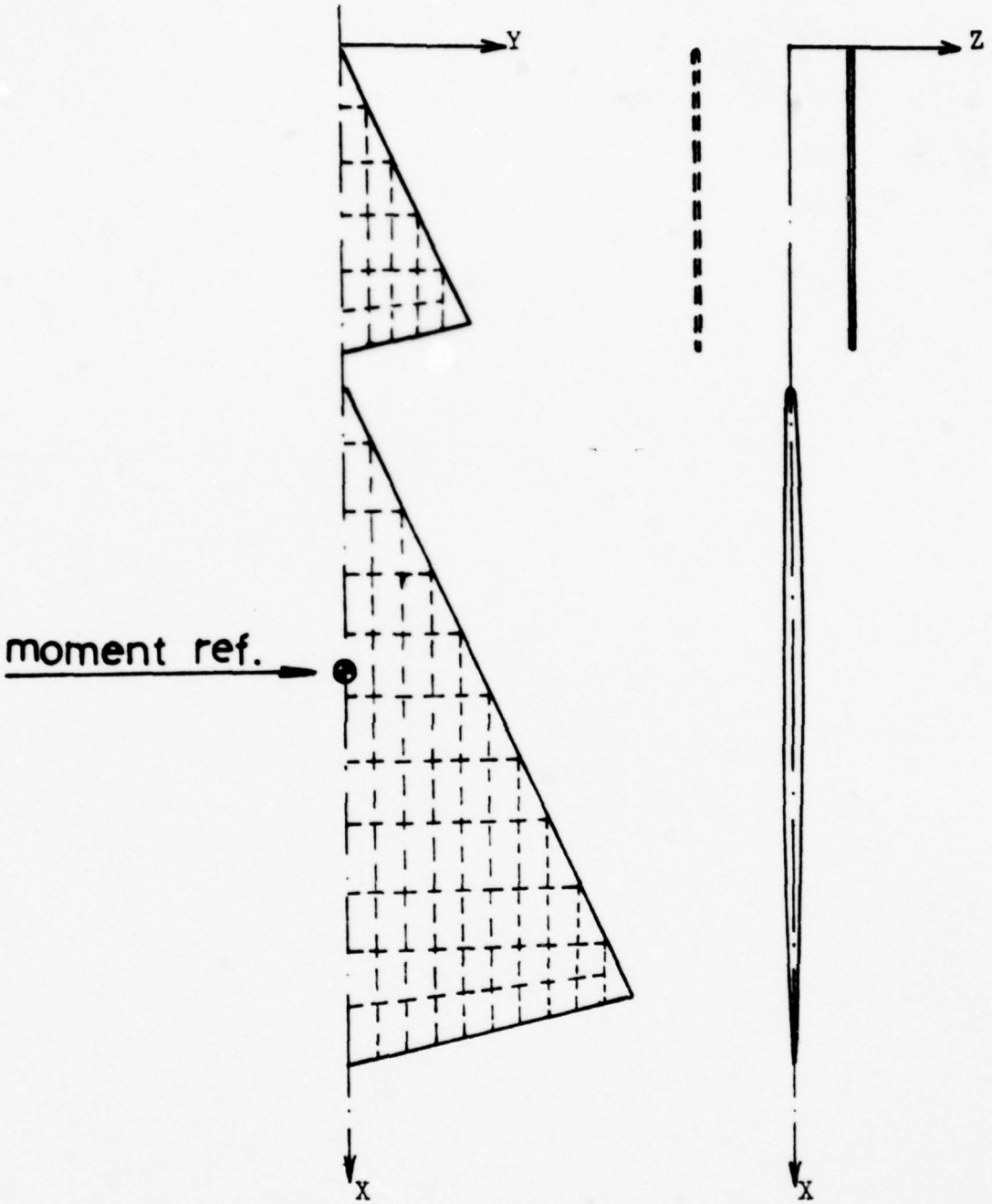

FIGURE 2 - COMPARISON WITH EXPERIMENTAL RESULTS - REF. 32; CANARD CONFIGURATION NO. 1 PARTITIONED INTO ELEMENTAL PANELS.

——————— FAIRED DATA CURVE (ROUND L.E.),HIGH CANARD

— · — · — PRESENT CALCULATION

— — — — MAX. LIFT PREDICTED BY PRESENT WORK FOR SHARP L.E.

---------- LINEAR THEORY

(EXPERIMENTAL DATA TAKEN FROM REF.32)

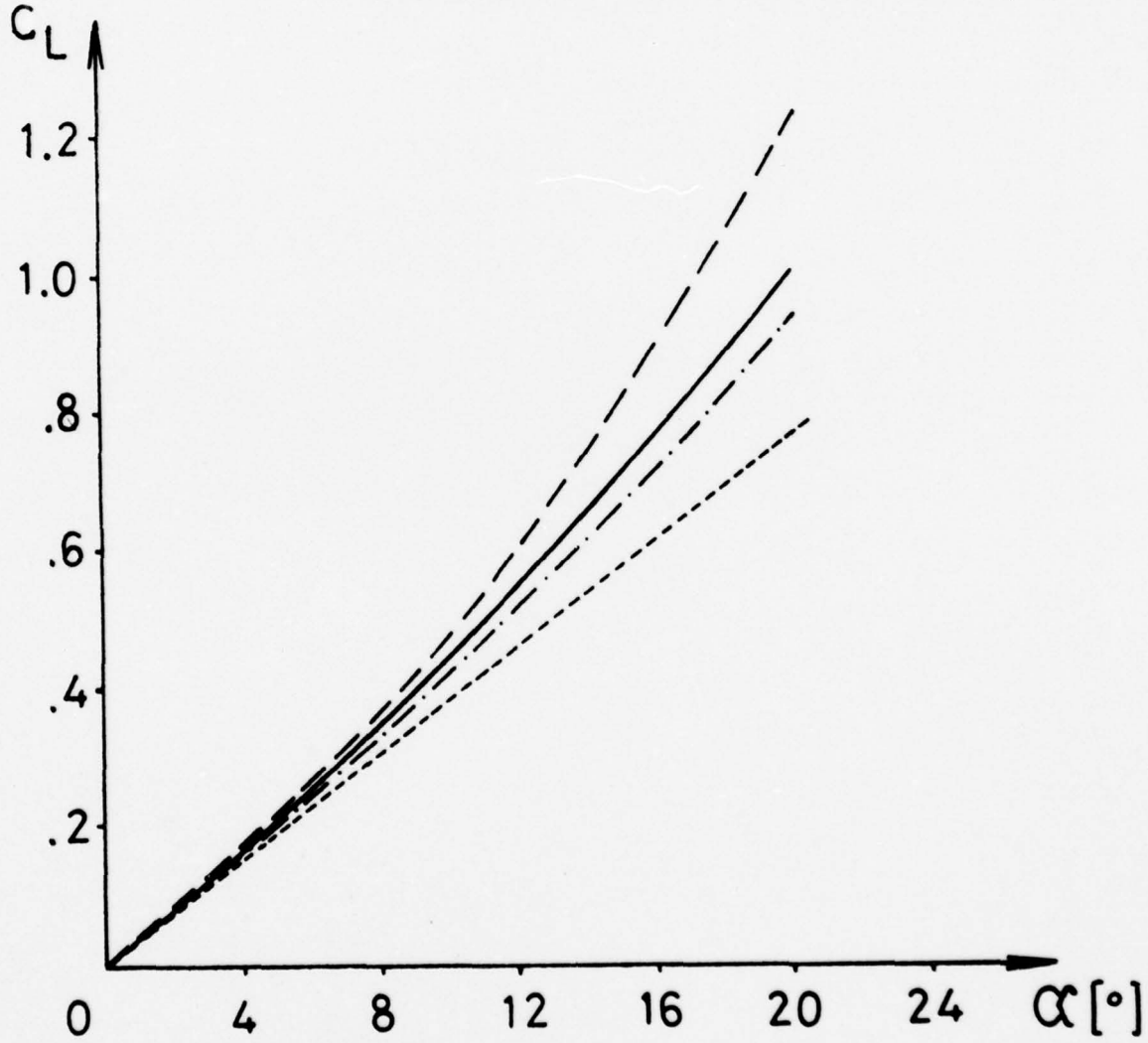

FIGURE 3-a - LIFT COEFFICIENT Vs. ANGLE OF ATTACK
FOR CONFIGURATION No. 1, HIGH CANARD.

——————— FAIRED DATA CURVE (ROUND L.E.),LOW CANARD

— — — — — FAIRED DATA CURVE (ROUND L.E.),HIGH CANARD

—·—·—·— PRESENT CALCULATION, LOW CANARD

---------- LINEAR THEORY

(EXPERIMENTAL DATA TAKEN FROM REF. 32)

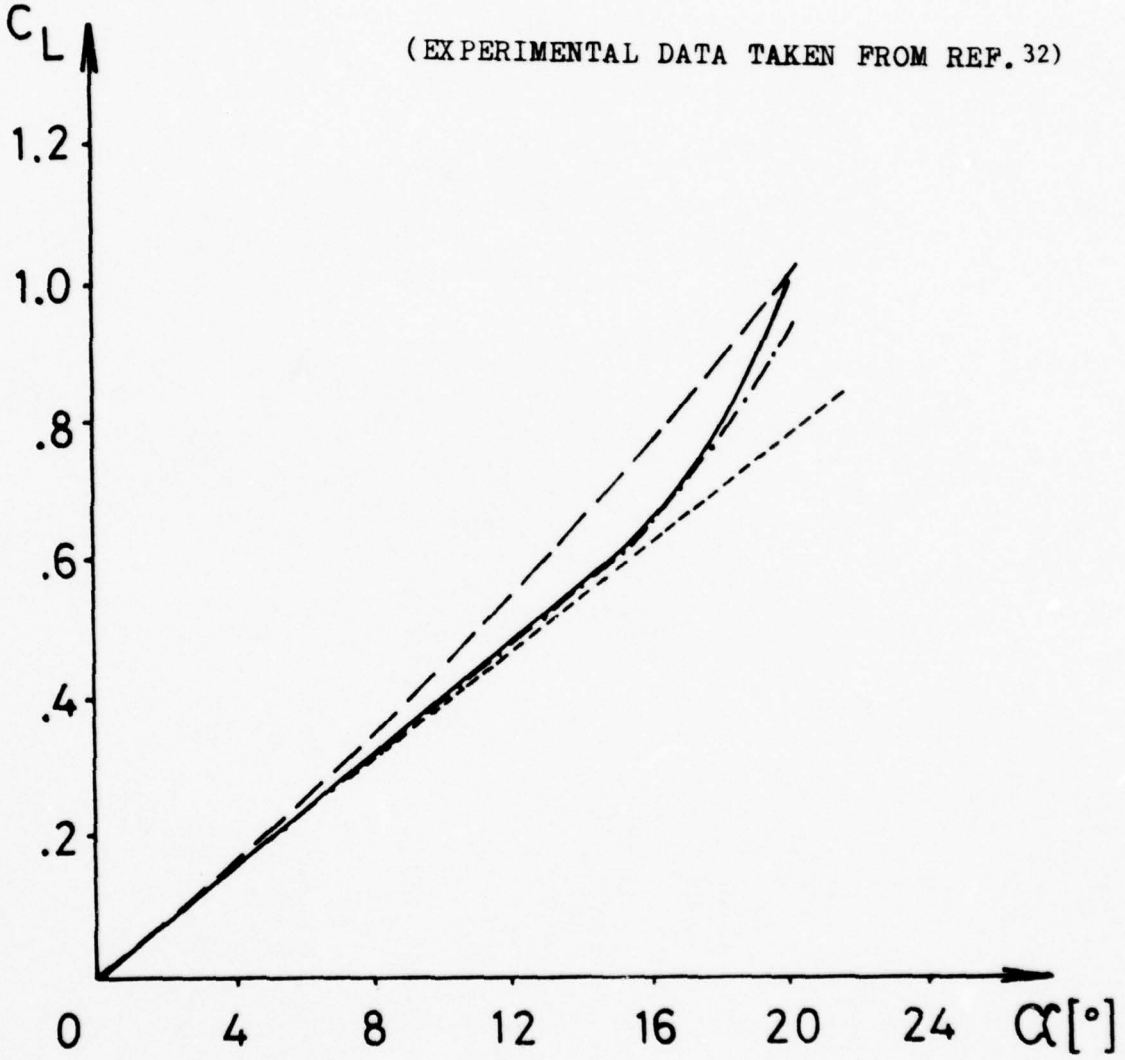

FIGURE 3-b - LIFT COEFFICIENT Vs. ANGLE OF ATTACK FOR CONFIGURATION No. 1, LOW CANARD.

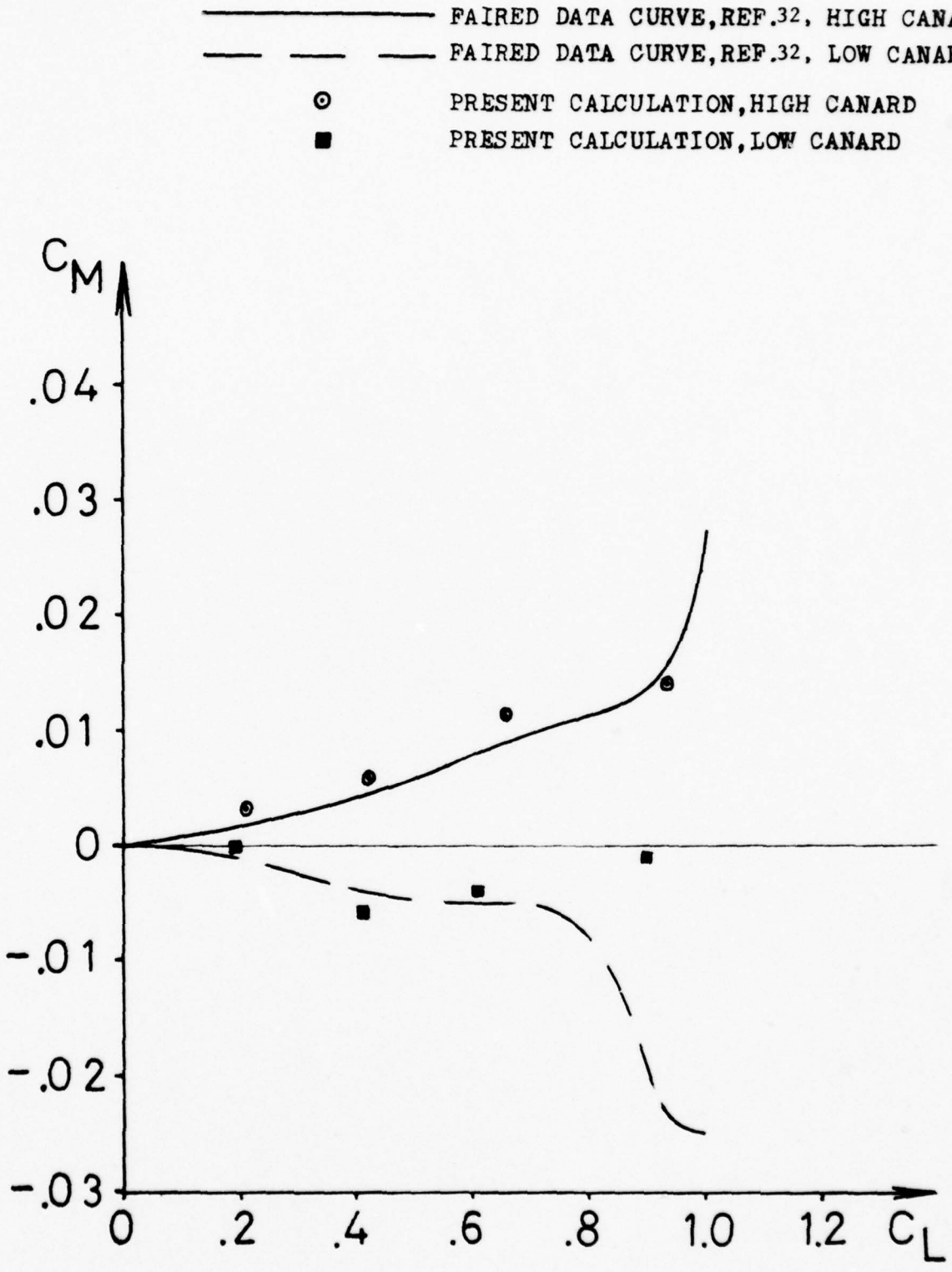

FIGURE 4 - PITCHING MOMENT COEFFICIENT Vs. LIFT COEFFICIENT FOR HIGH AND LOW CANARDS, CONFIGURATION No. 1.

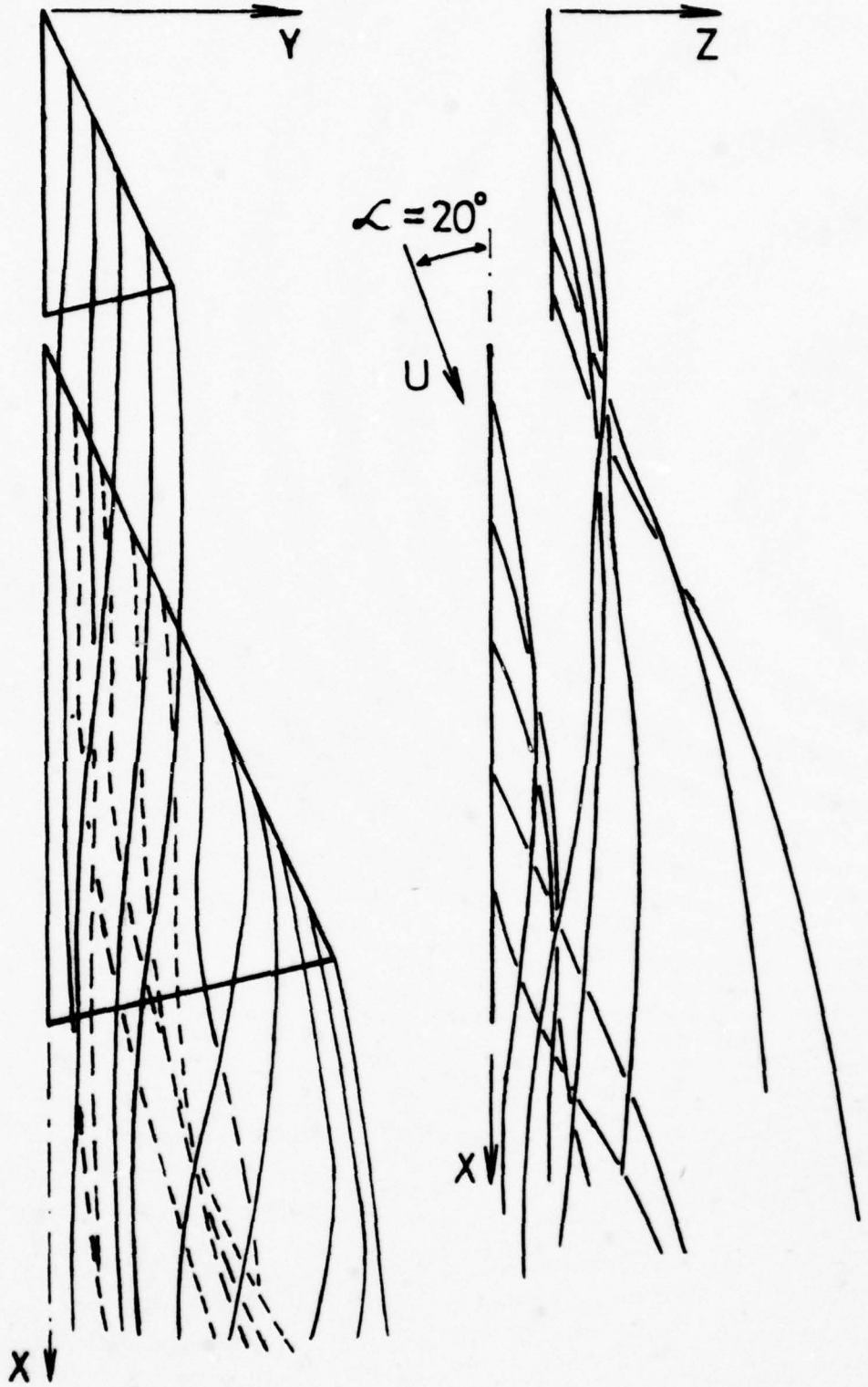

FIGURE 5 - CALCULATED INTERACTION BETWEEN CANARD AND WING LEADING EDGE VORTICES, CONFIGURATION NO. 1.

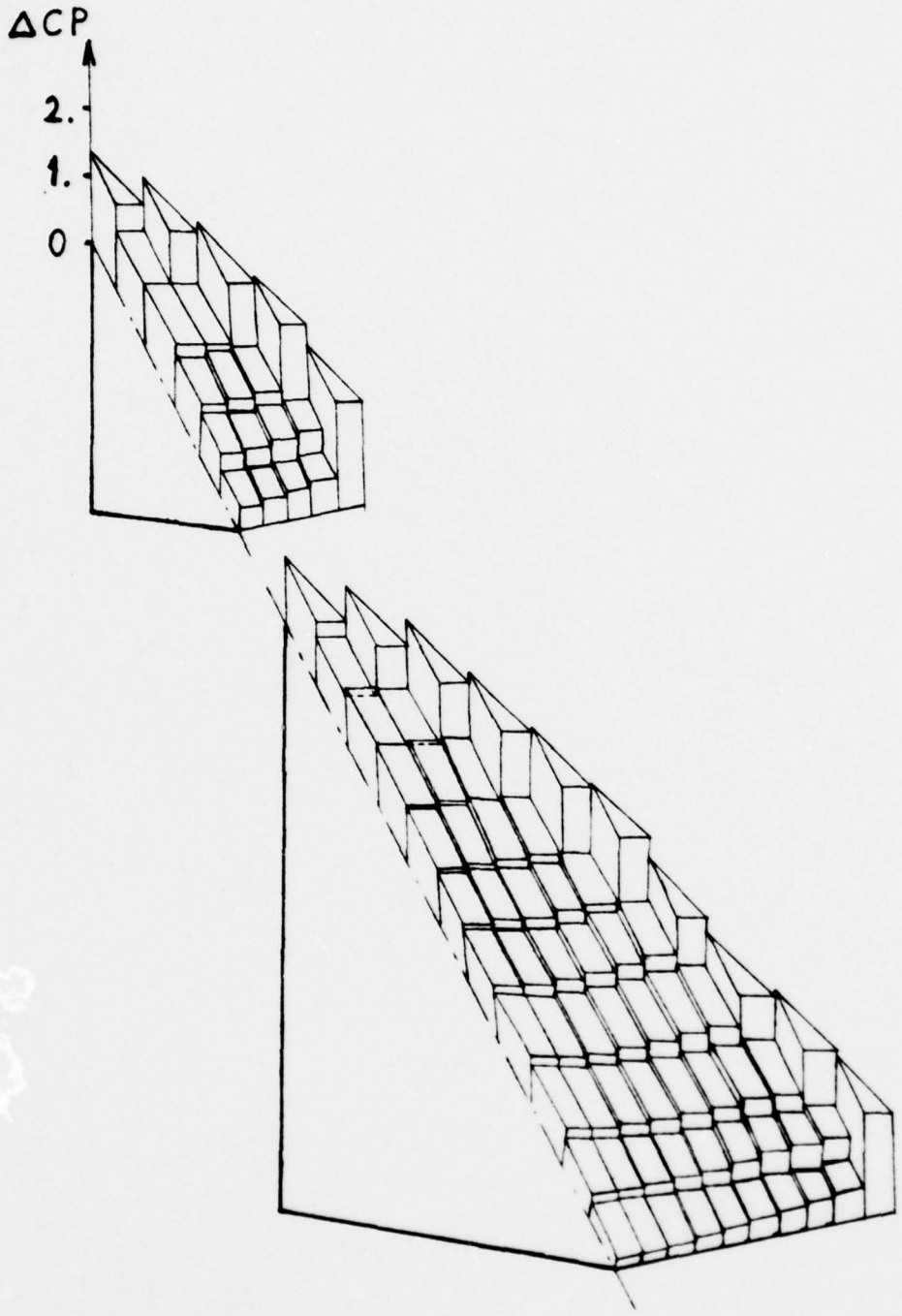

FIGURE 6 - AN EXAMPLE OF CALCULATED LOAD DISTRIBUTION OF WING AND CANARD AT 20 DEG. ANGLE OF ATTACK, CONFIGURATION NO. 1.

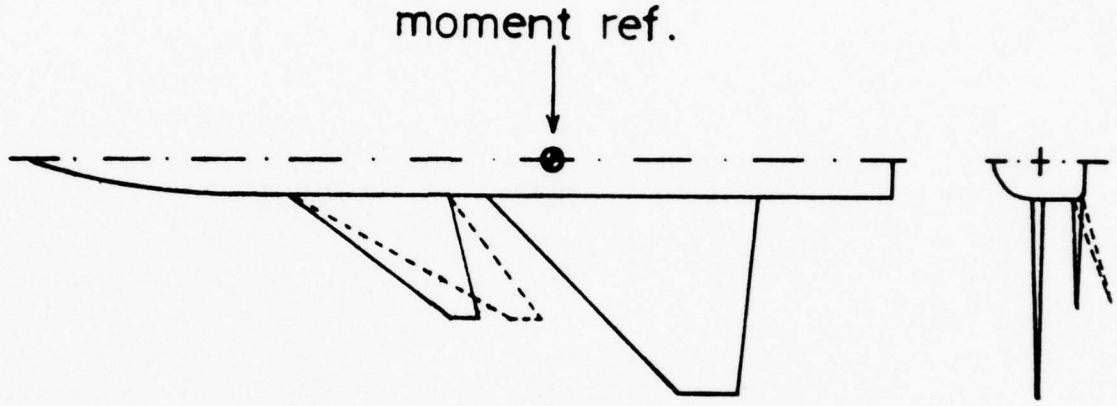

CONFIG. NO.2 : 51.7° CANARD L.E. SWEEP, 0° DIHEDRAL

CONFIG. NO.3 : 51.7° CANARD L.E. SWEEP, 18.6° DIHEDRAL

CONFIG. NO.4 : 60° CANARD L.E. SWEEP, 0° DIHEDRAL

FIGURE 7 - COMPARISON WITH EXPERIMENTAL RESULTS - REF. 33 , WING CANARD CONFIGURATIONS Nos. 2, 3, 4.

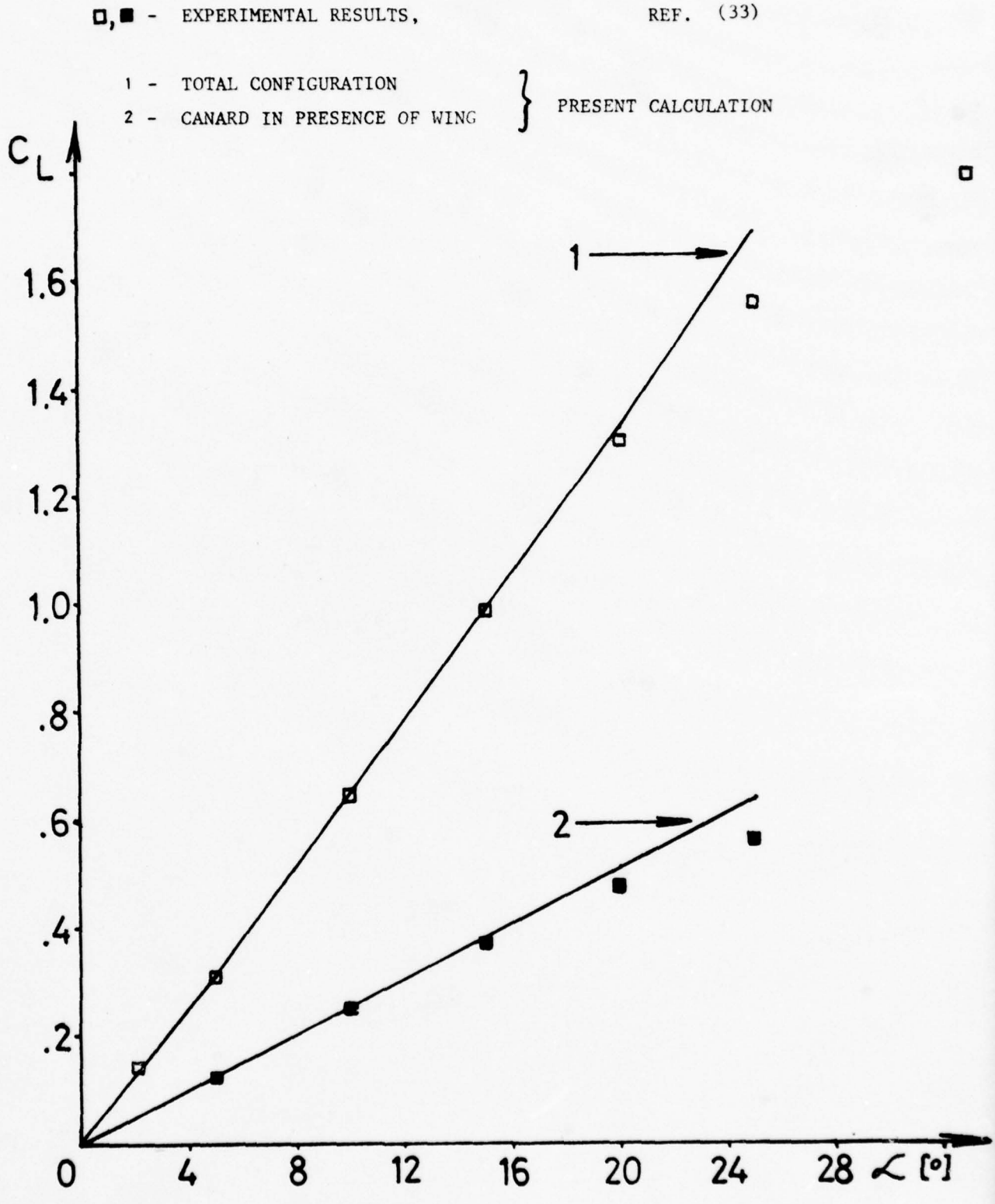

FIGURE 8 - LIFT COEFFICIENT Vs. ANGLE OF ATTACK, CONFIGURATION No. 2.

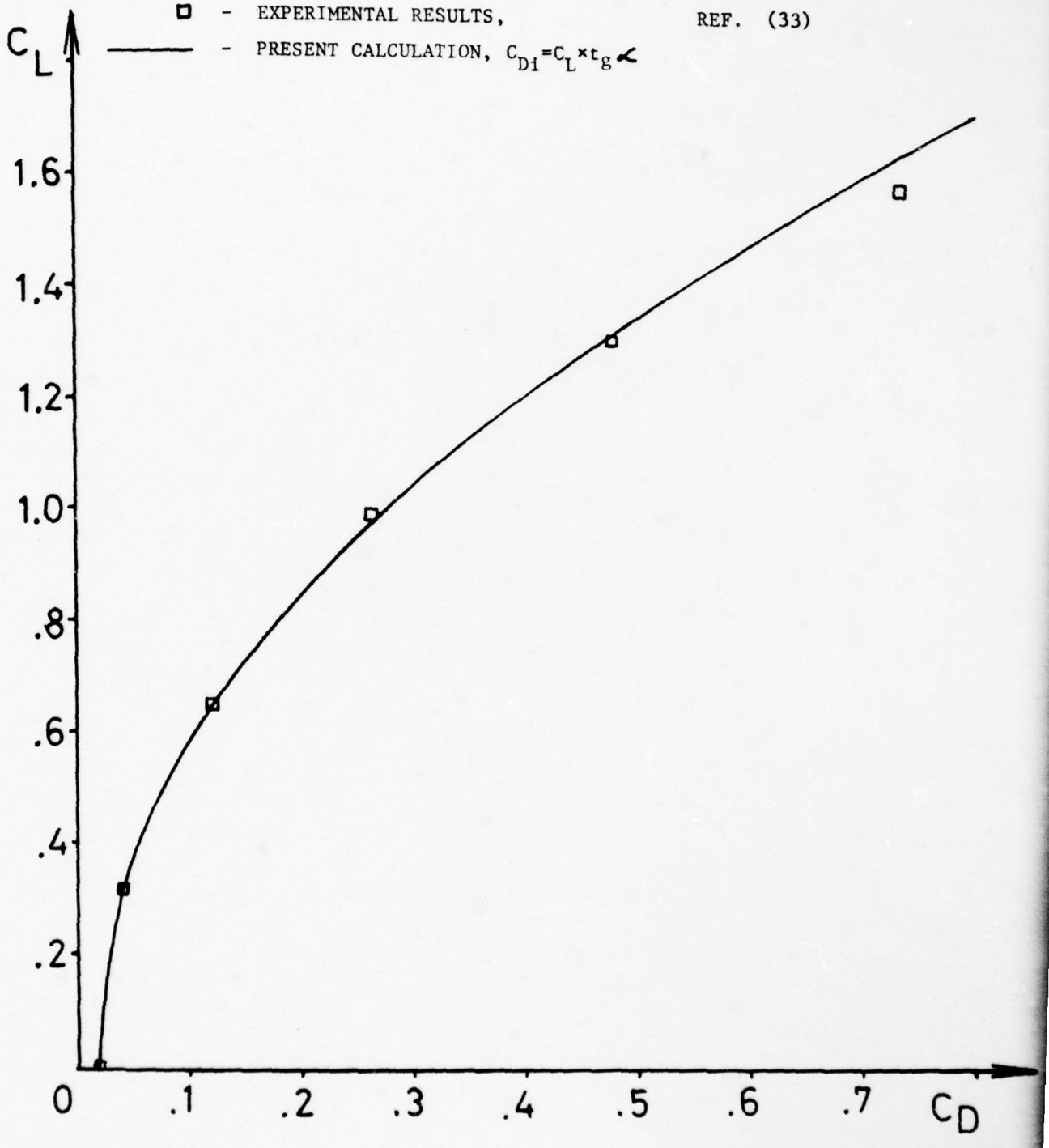

FIGURE 9 - LIFT COEFFICIENT Vs. DRAG COEFFICIENT, CONFIGURATION No. 2.

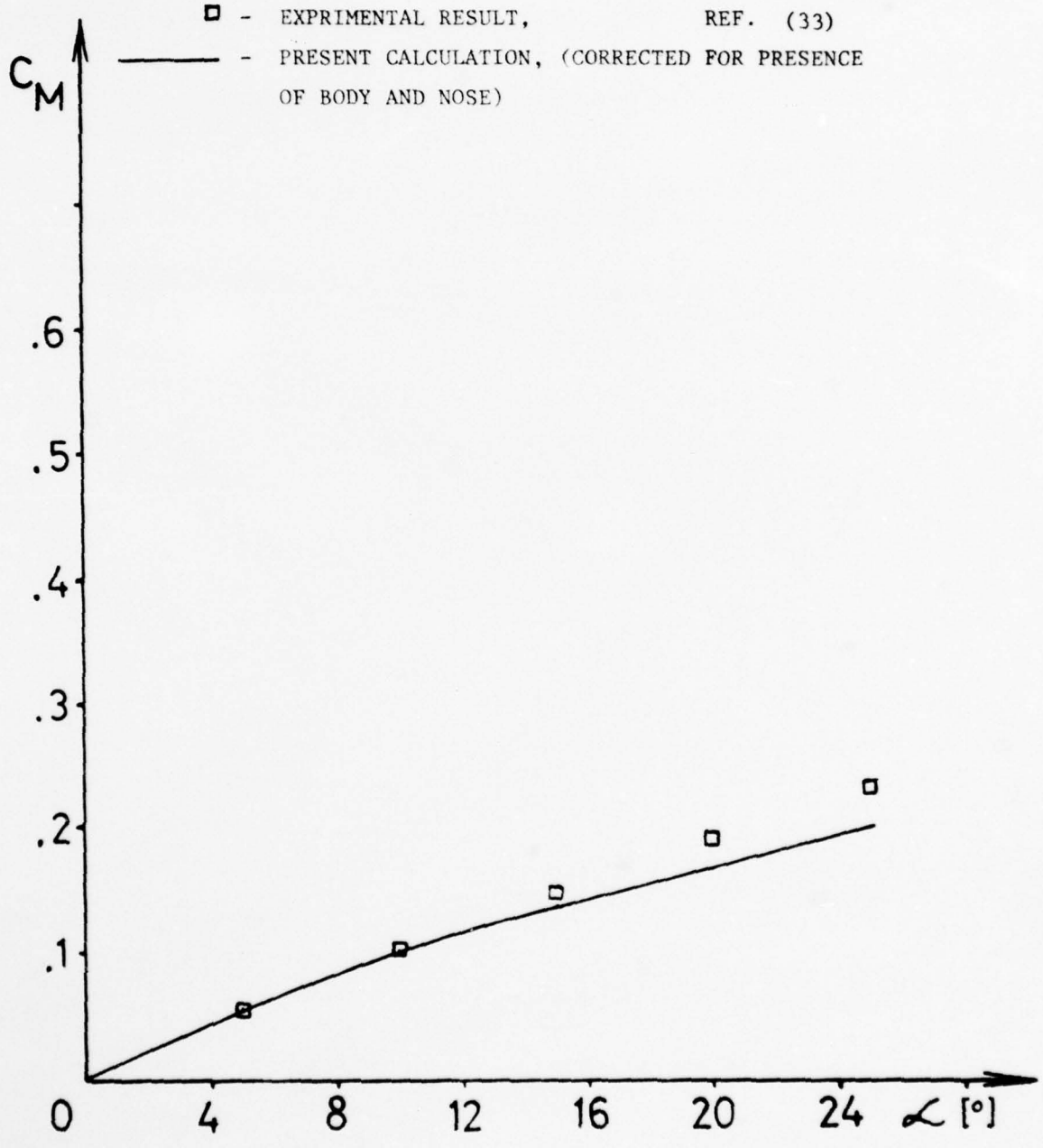

FIGURE 10 - PITCHING MOMENT COEFFICIENT Vs. ANGLE OF ATTACK, CONFIGURATION No. 2

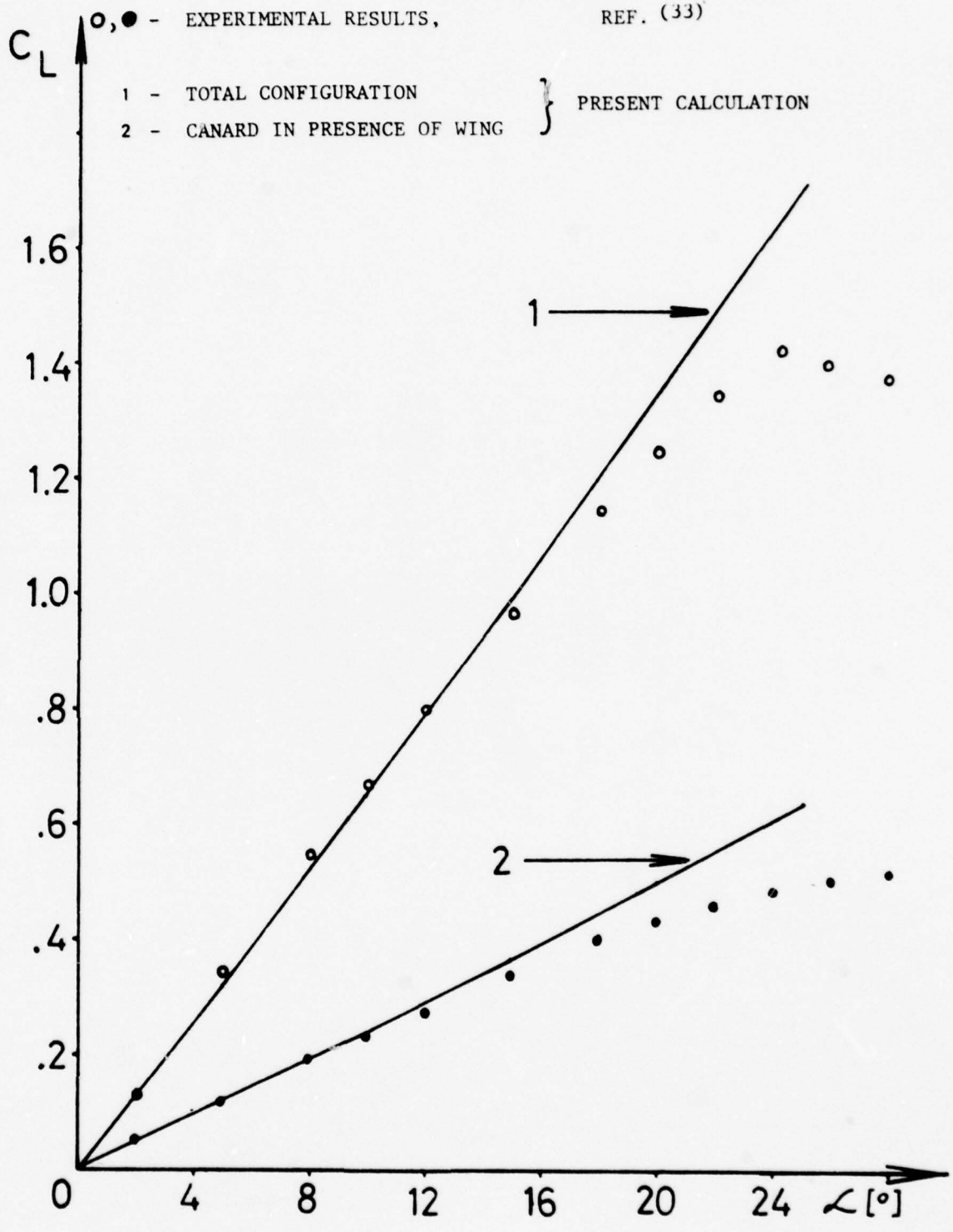

FIGURE 11 - LIFT COEFFICIENT Vs. ANGLE OF ATTACK, CONFIGURATION No. 3.

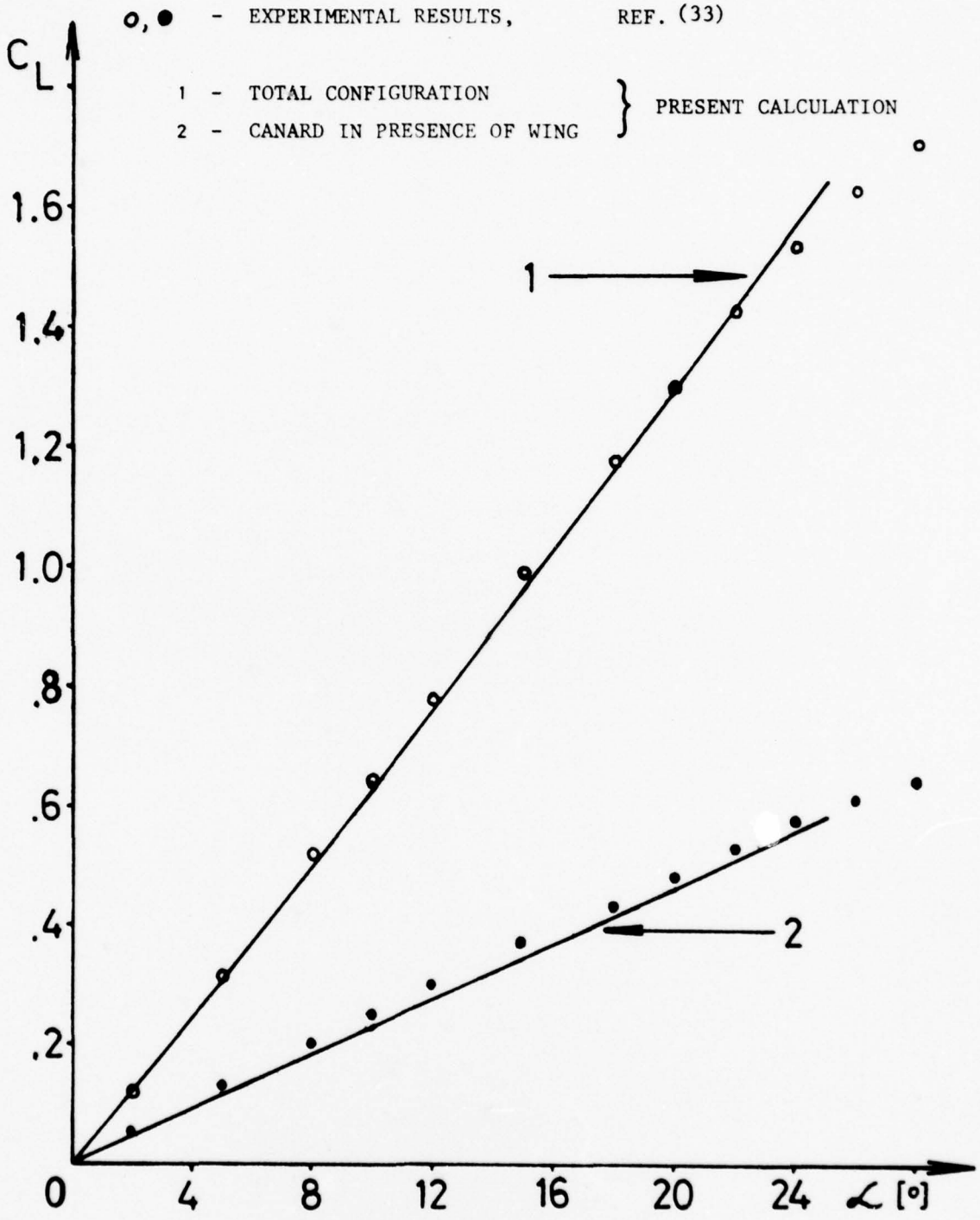

FIGURE 12 - LIFT COEFFICIENT Vs. ANGLE OF ATTACK, CONFIGURATION No. 4.

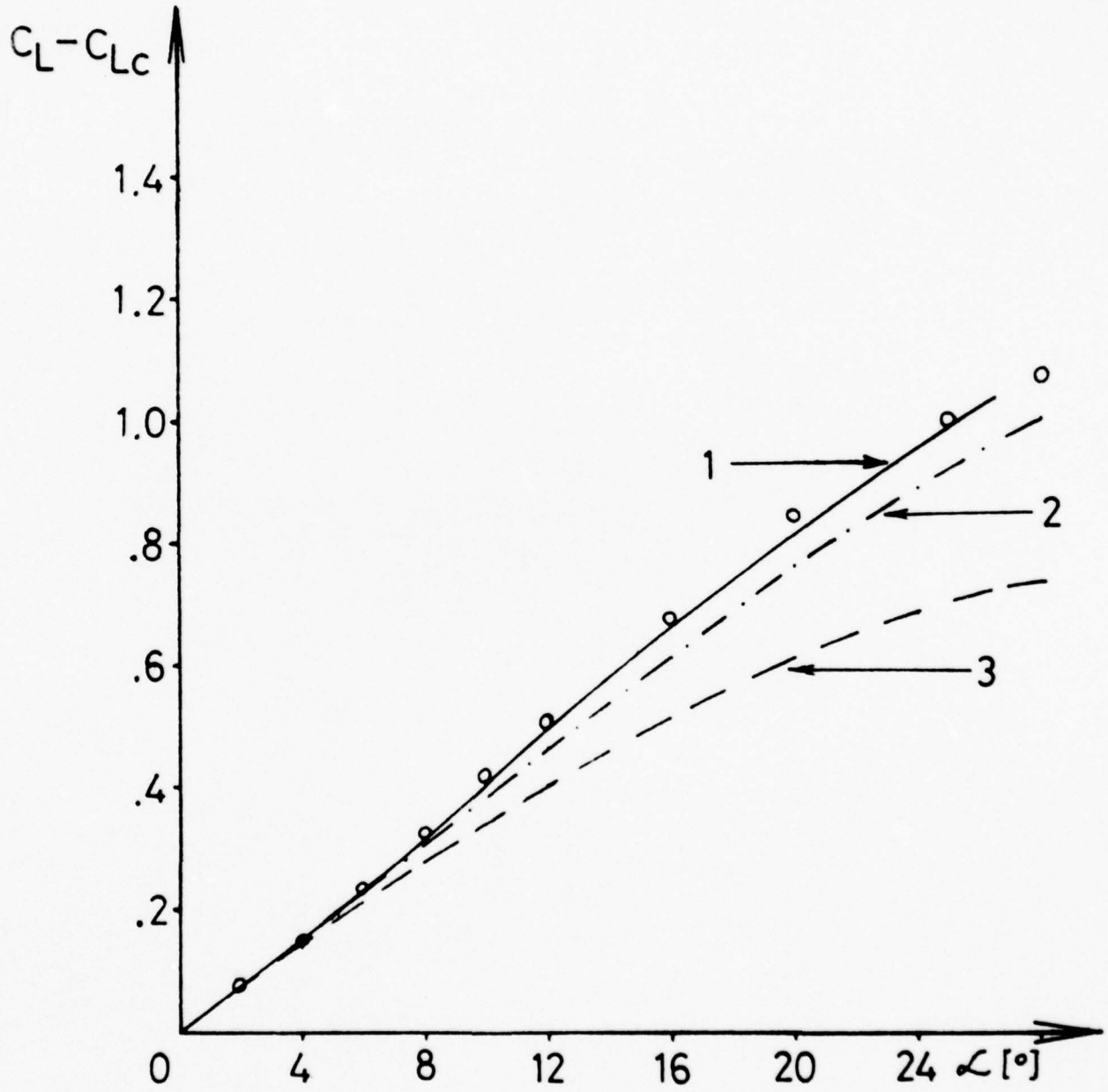

FIGURE 13 - COMPARISON OF EXPERIMENTAL RESULTS TO VARIOUS THEORETICAL RESULTS FOR CONFIGURATION No. 2.

CANARD IN PRESENCE OF WING :

O - EXPERIMENTAL RESULTS, REF. (33)

1 - PRESENT CALCULATION

2 - $C_{Lp} + C_{Lv}$,(MODIFIED POLHAMUS), REF. (33)

3 - C_{Lp} , (MODIFIED POLHAMUS), REF. (33)

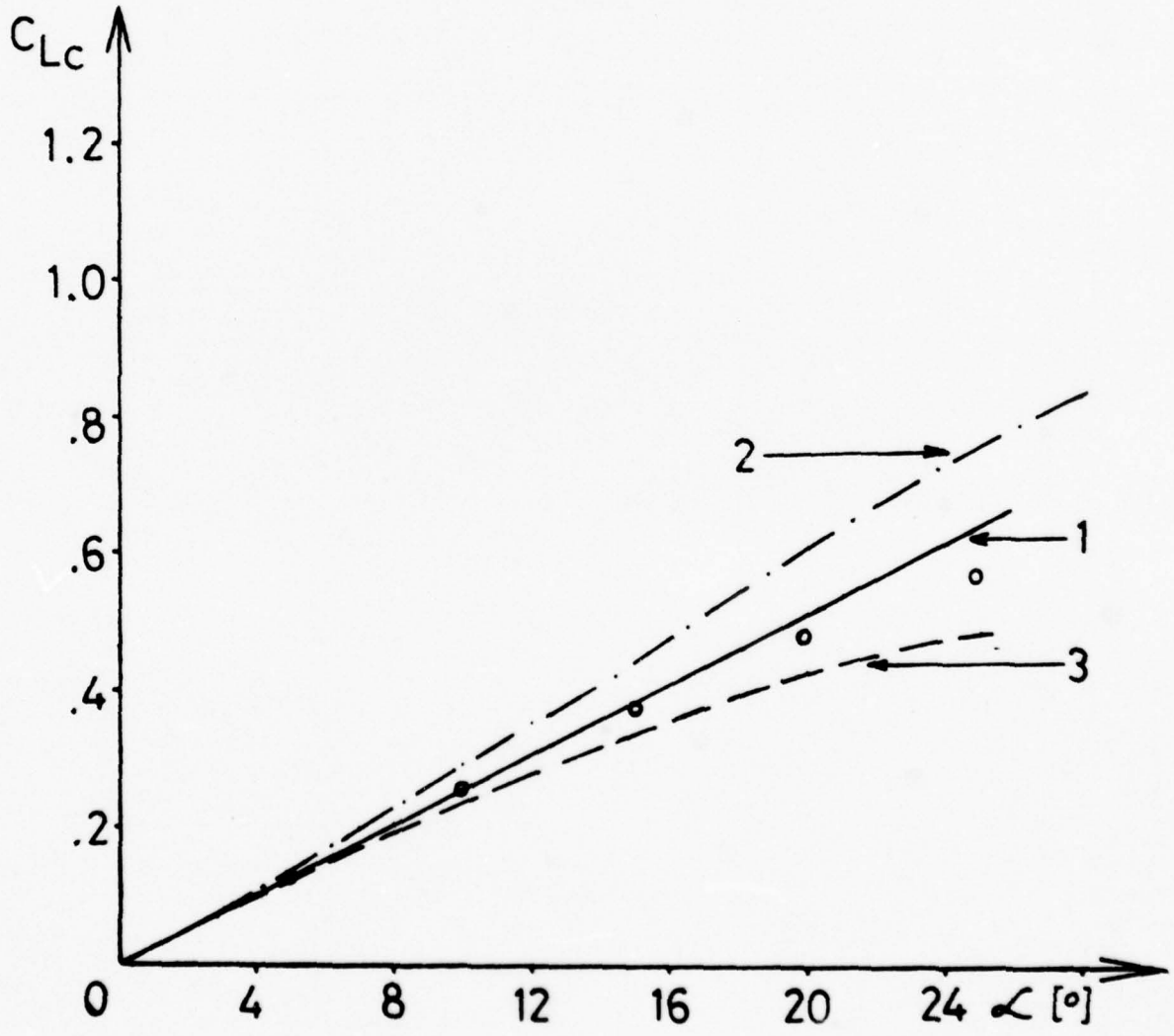

FIGURE 14 - COMPARISON OF EXPERIMENTAL RESULTS TO VARIOUS THEORETICAL RESULTS FOR CONFIGURATION No.2.

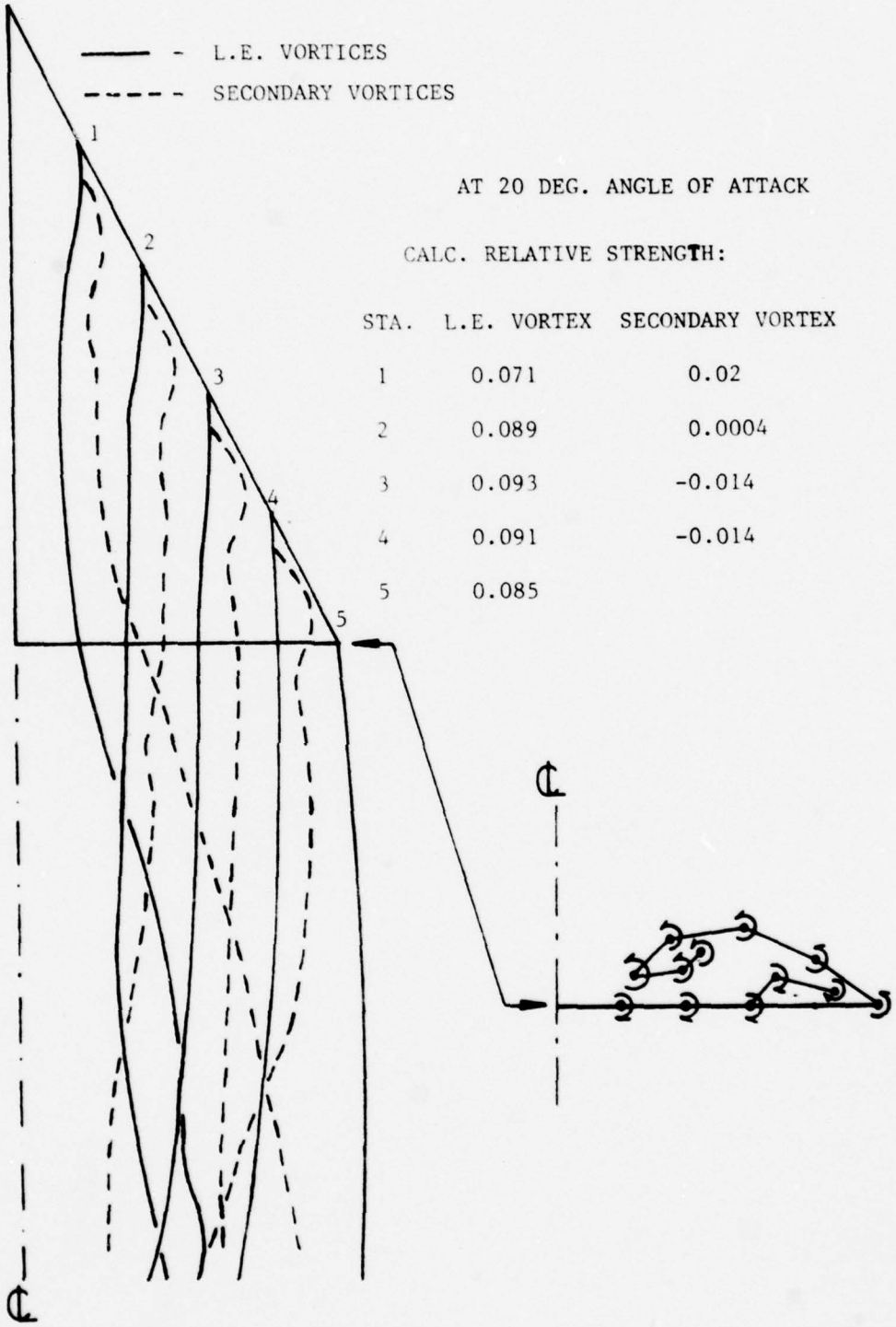

AT 20 DEG. ANGLE OF ATTACK

CALC. RELATIVE STRENGTH:

STA.	L.E. VORTEX	SECONDARY VORTEX
1	0.071	0.02
2	0.089	0.0004
3	0.093	-0.014
4	0.091	-0.014
5	0.085	

FIG. 15 : LEADING EDGE VORTICES AND SECONDARY VORTICES CALCULATED FOR AR=2 DELTA WING

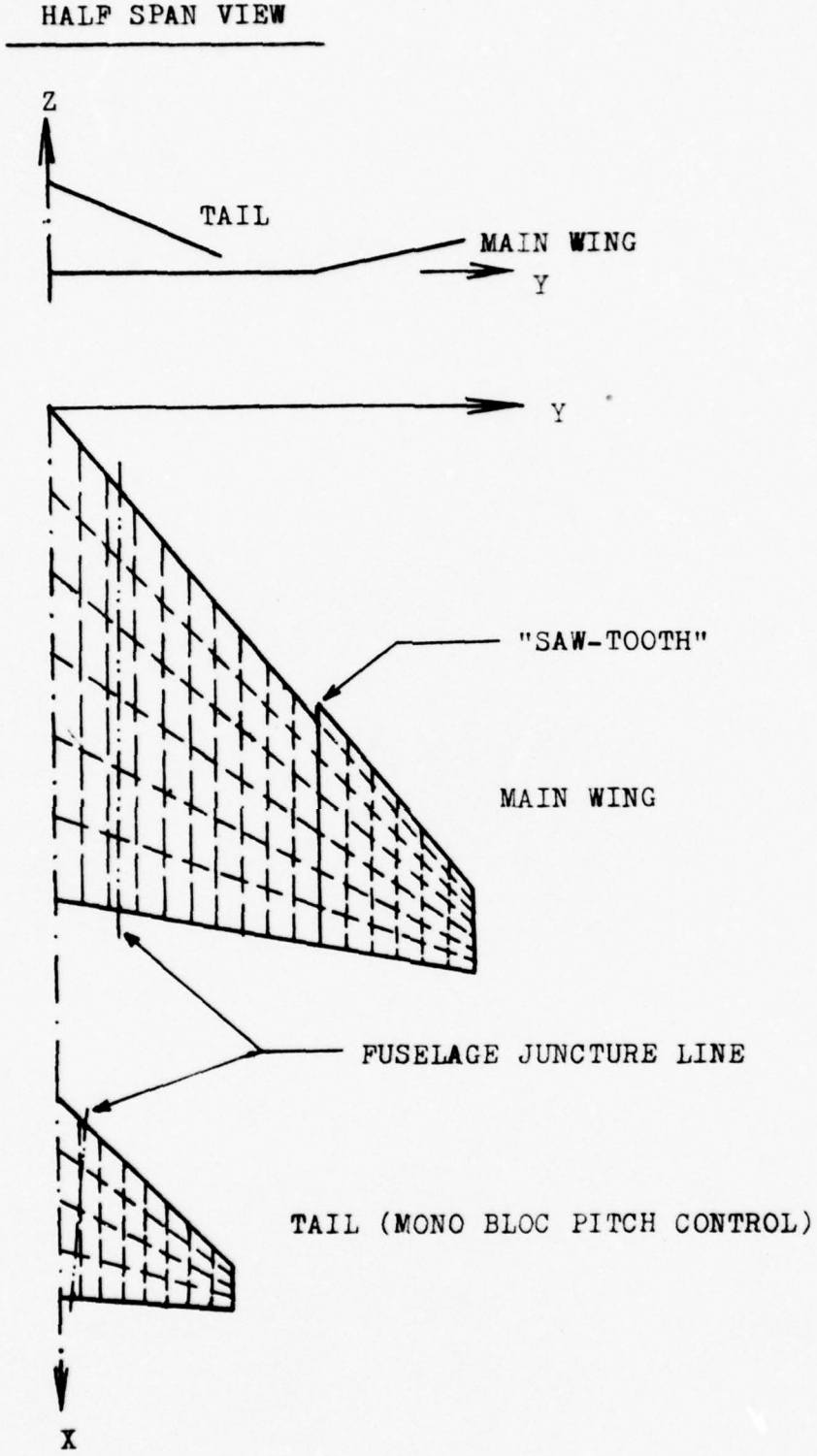

FIGURE 16 - SCHEMATIC DESCRIPTION OF THE MODEL OF AN F-4-E PARTITIONED INTO ELEMENTAL PANELS.

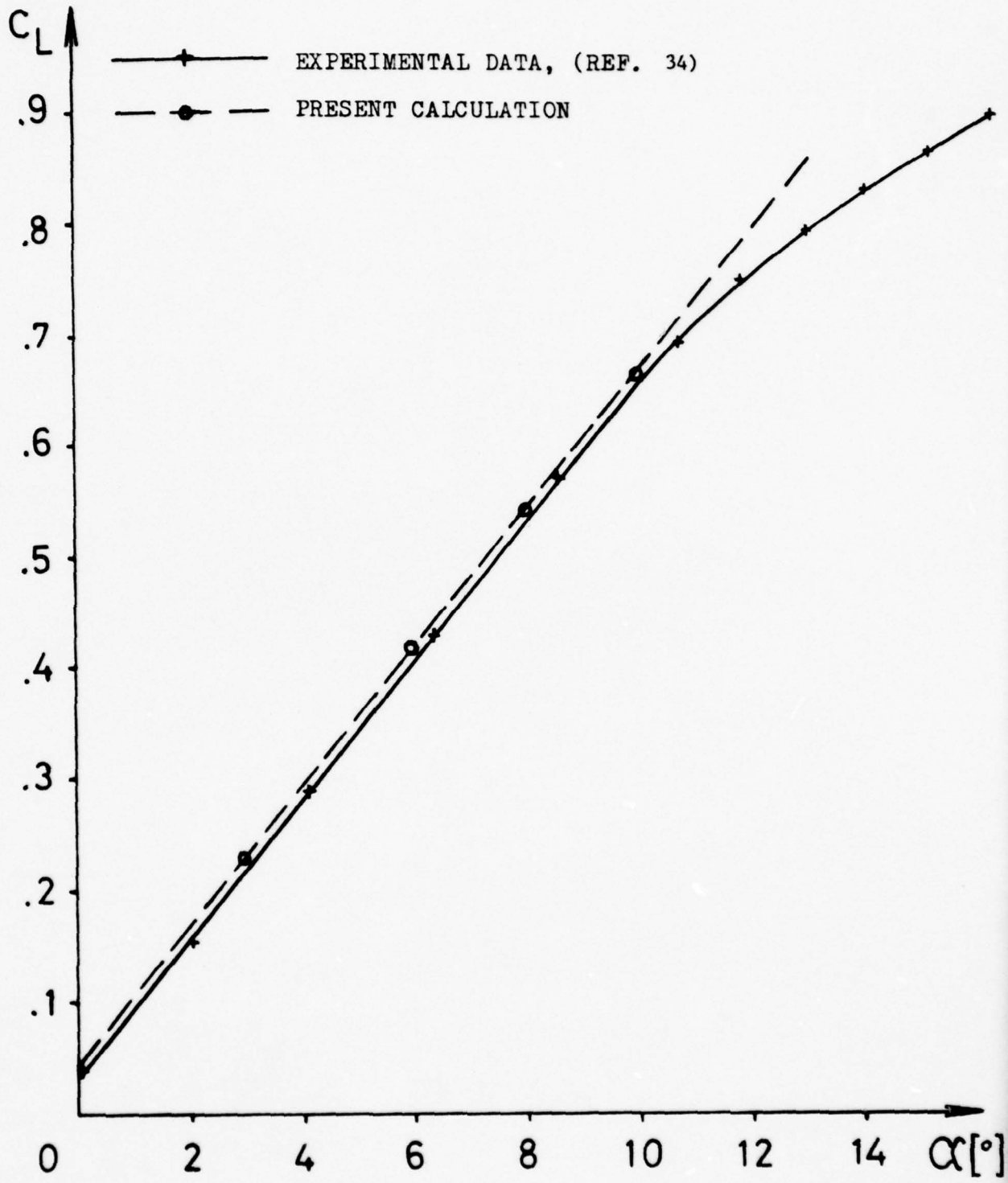

FIGURE 17 - LIFT COEFFICIENT Vs. ANGLE OF ATTACK, F-4-E MODEL, AT 0.6 MACH NUMBER.

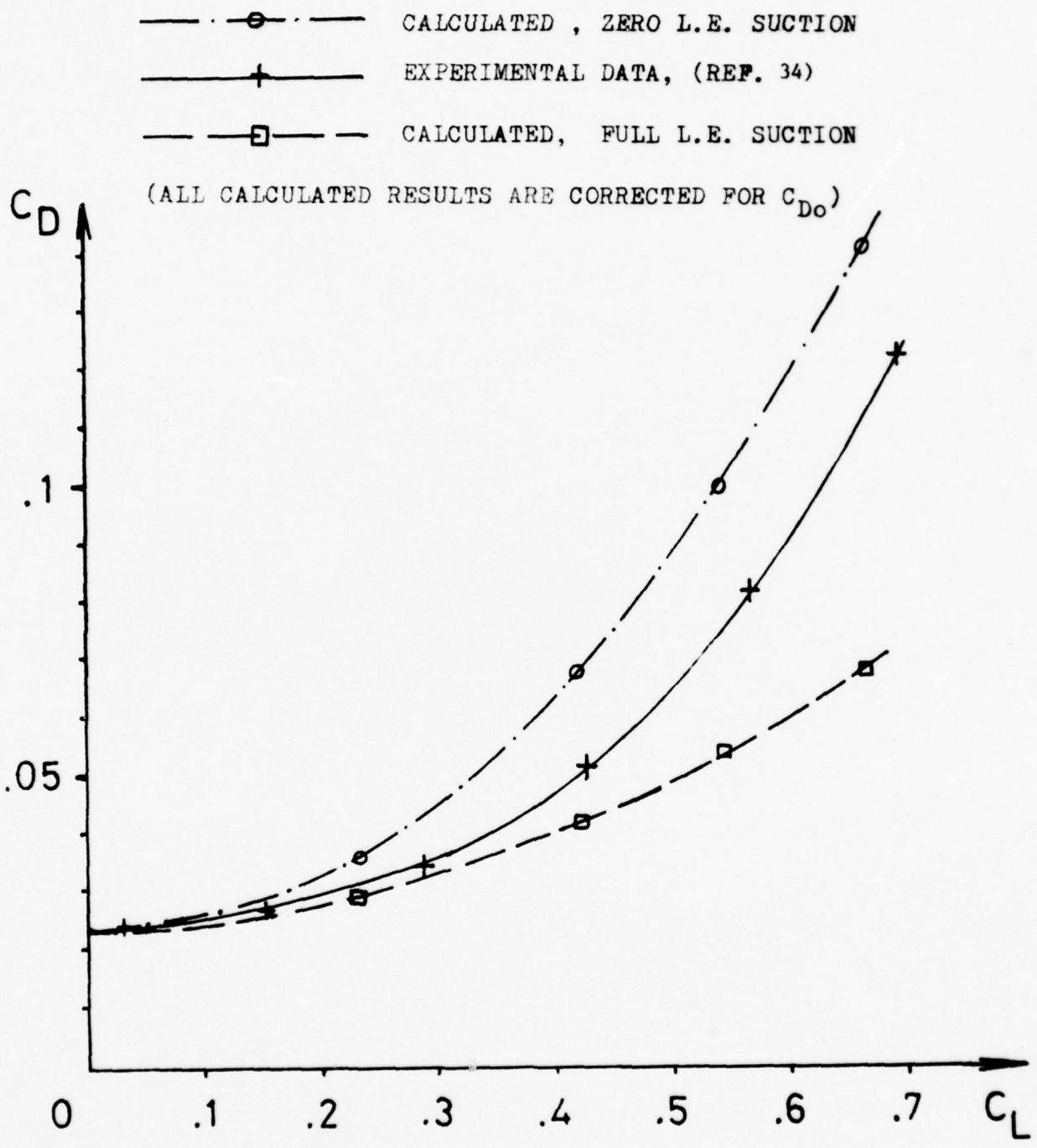

FIGURE 18 - TOTAL DRAG COEFFICIENT Vs. LIFT COEFFICIENT, F-4-E MODEL AT 0.6 MACH NUMBER.

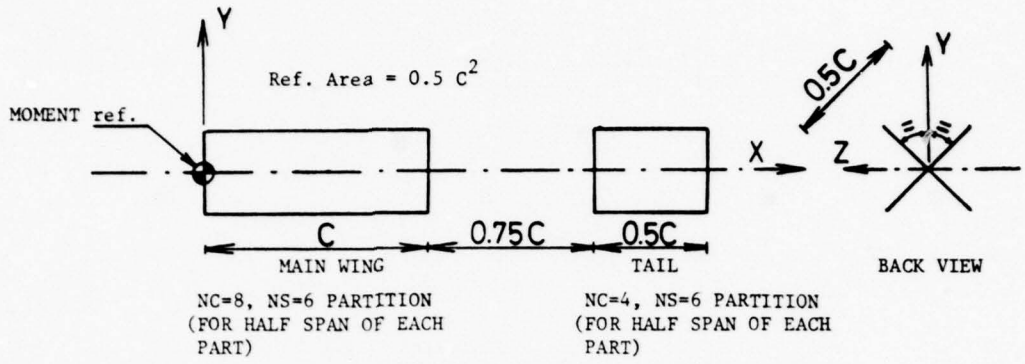

FIG. 19 - DESCRIPTION OF THE CRUCIFORM MODEL

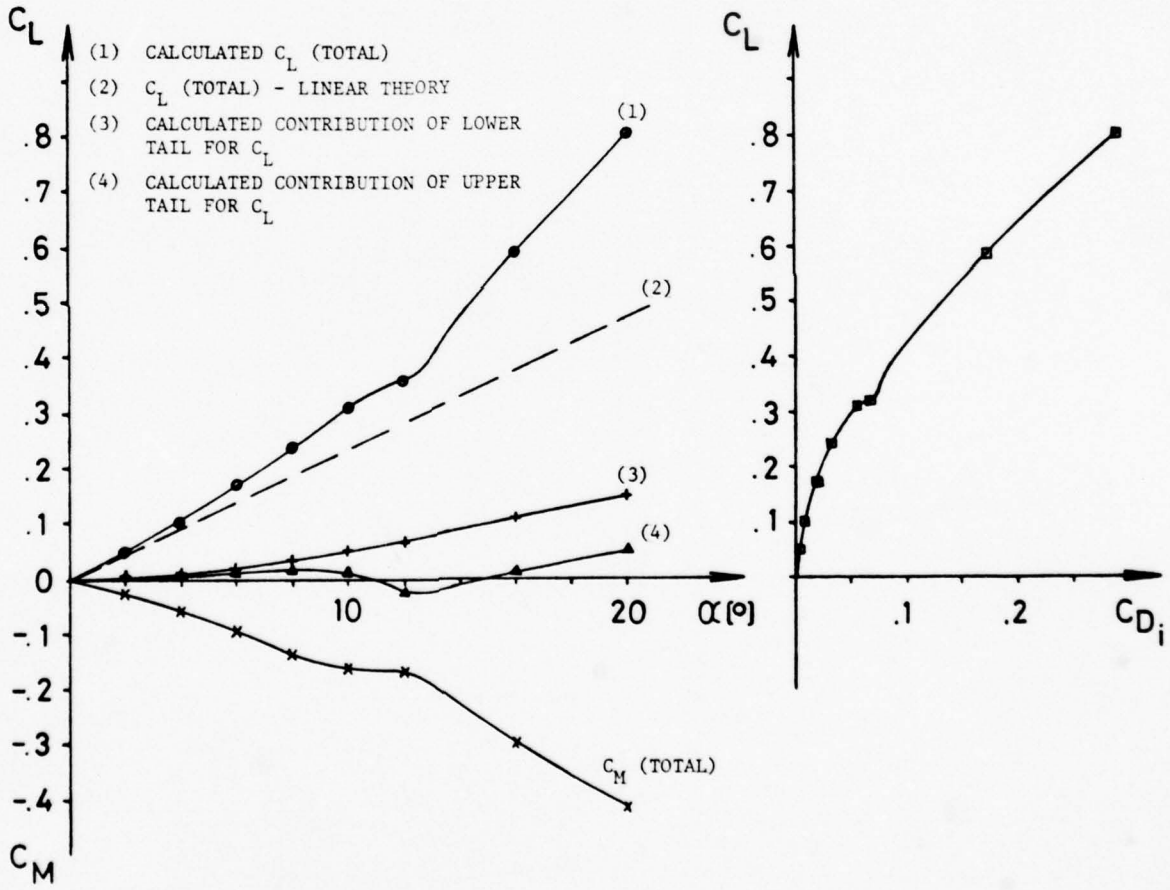

FIG. 20 - LIFT AND PITCHING MOMENT COEFFICIENTS Vs. ANGLE OF ATTACK; INDUCED DRAG COEFFICIENT Vs. LIFT COEFFICIENT, CALCULATED FOR THE CRUCIFORM CONFIGURATION

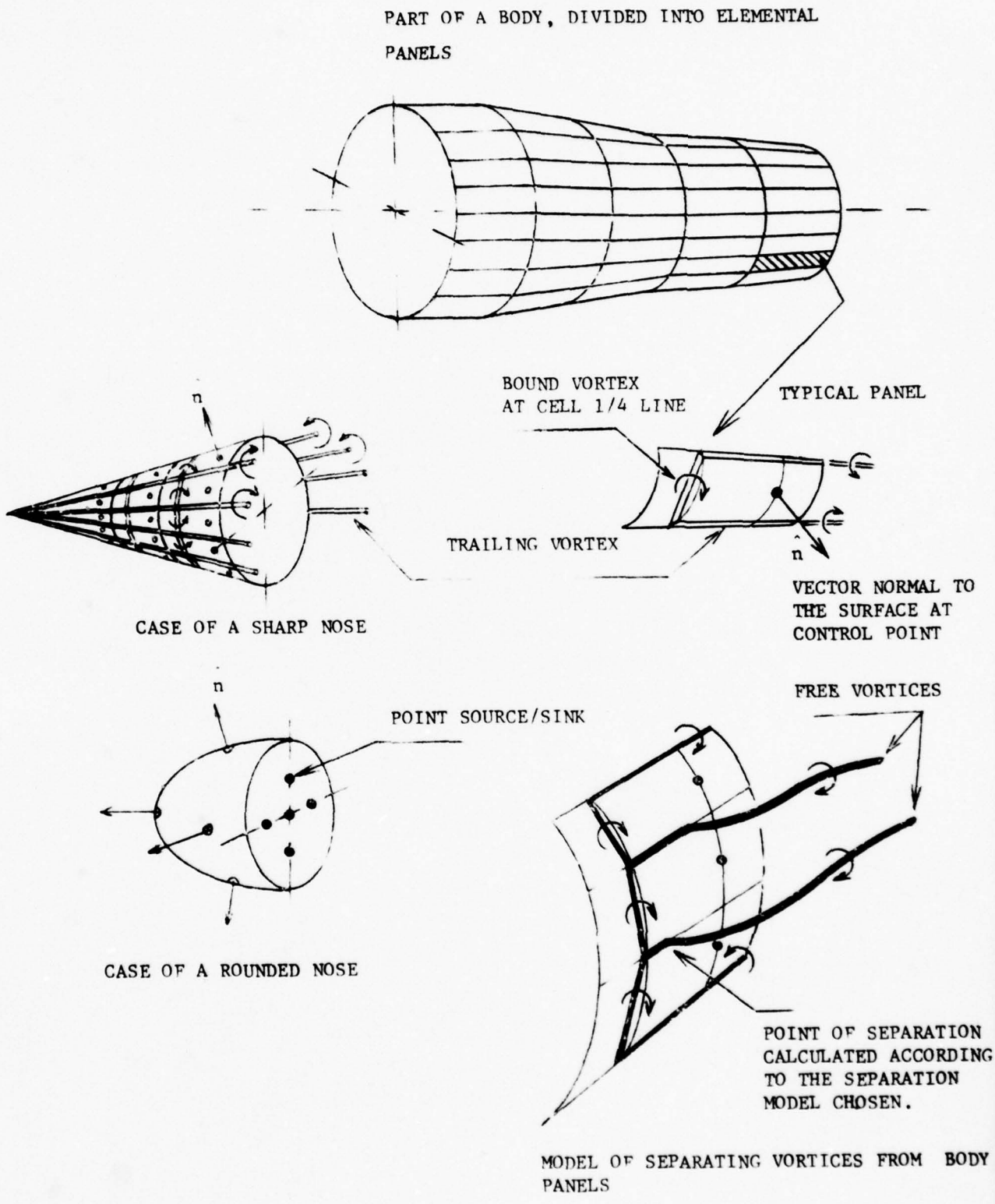

FIG. 21 - PROPOSED MODEL FOR A BODY INCLUDING VORTEX SEPARATION

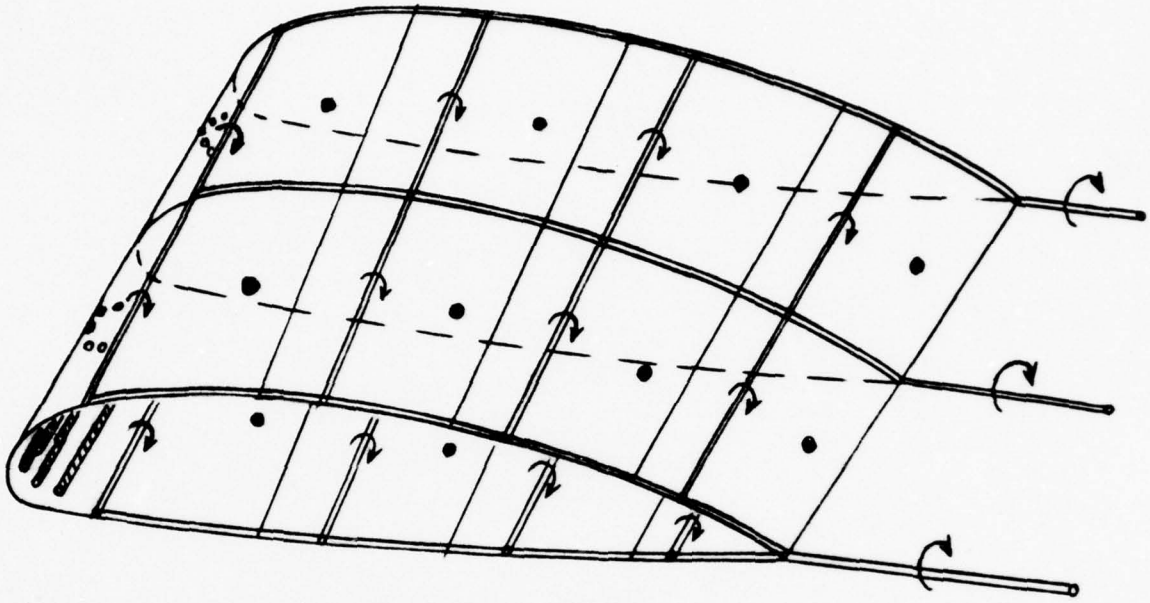

ORDINARY CASE OF A THICK WING

ELEMENTAL PANEL PERIMETER

BOUND AND TRAILING VORTICES

LINE SOURCES/SINKS

CONTROL POINTS

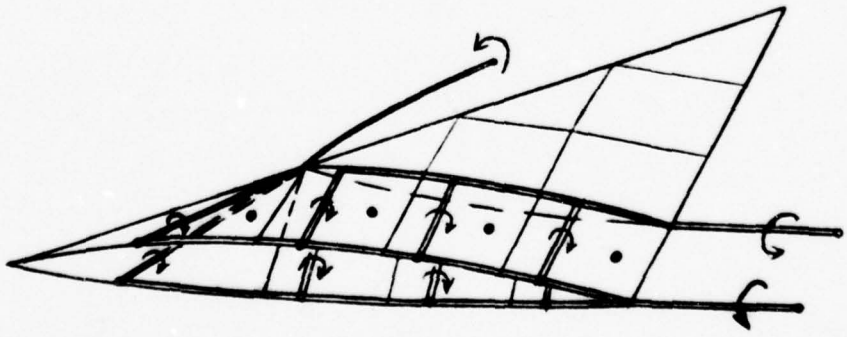

CASE OF L.E. SEPARATION

Fig. 22 - PROPOSED MODEL FOR THICK WINGS

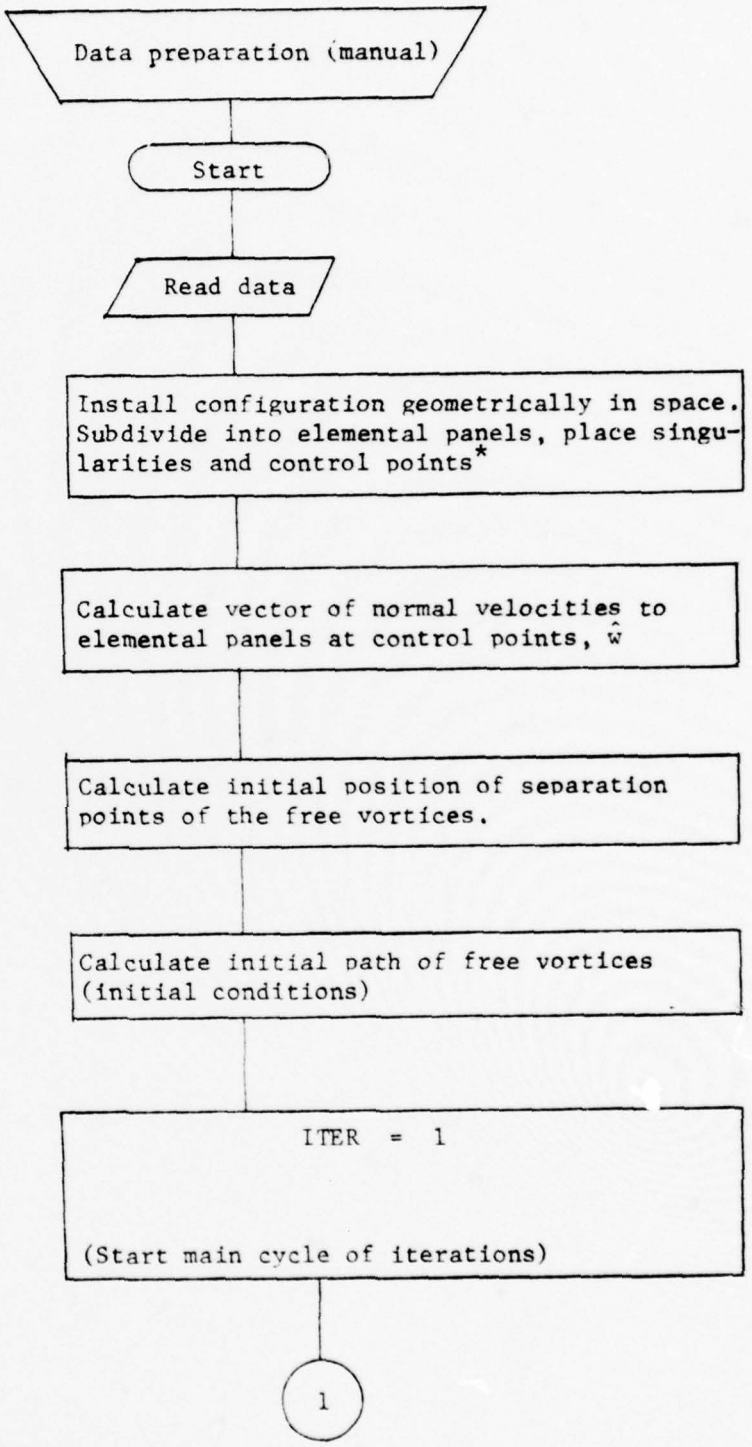

FIGURE 23 - SCHEMATIC FLOW-CHART OF THE CALCULATION, (PRESENT METHOD).

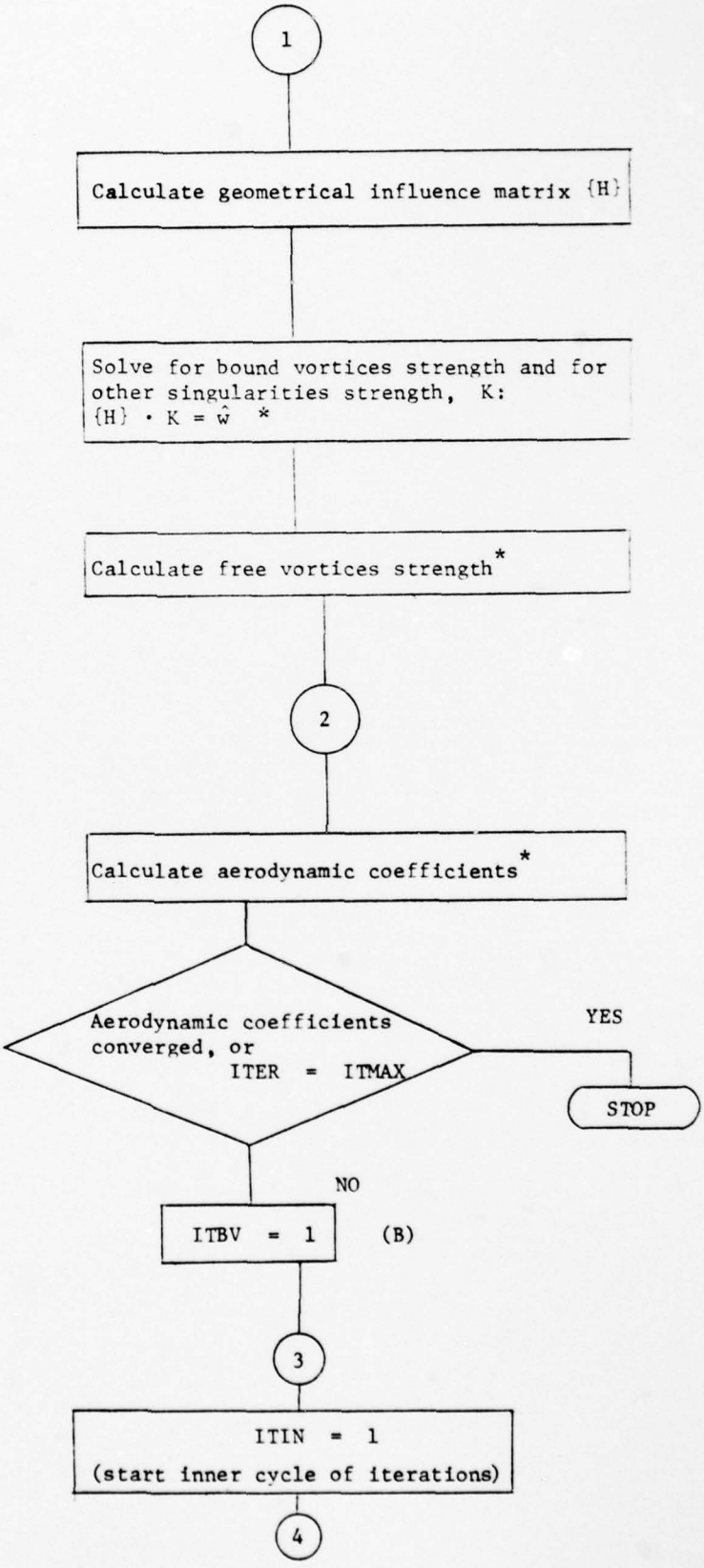

FIG. 23 (CONTINUED)

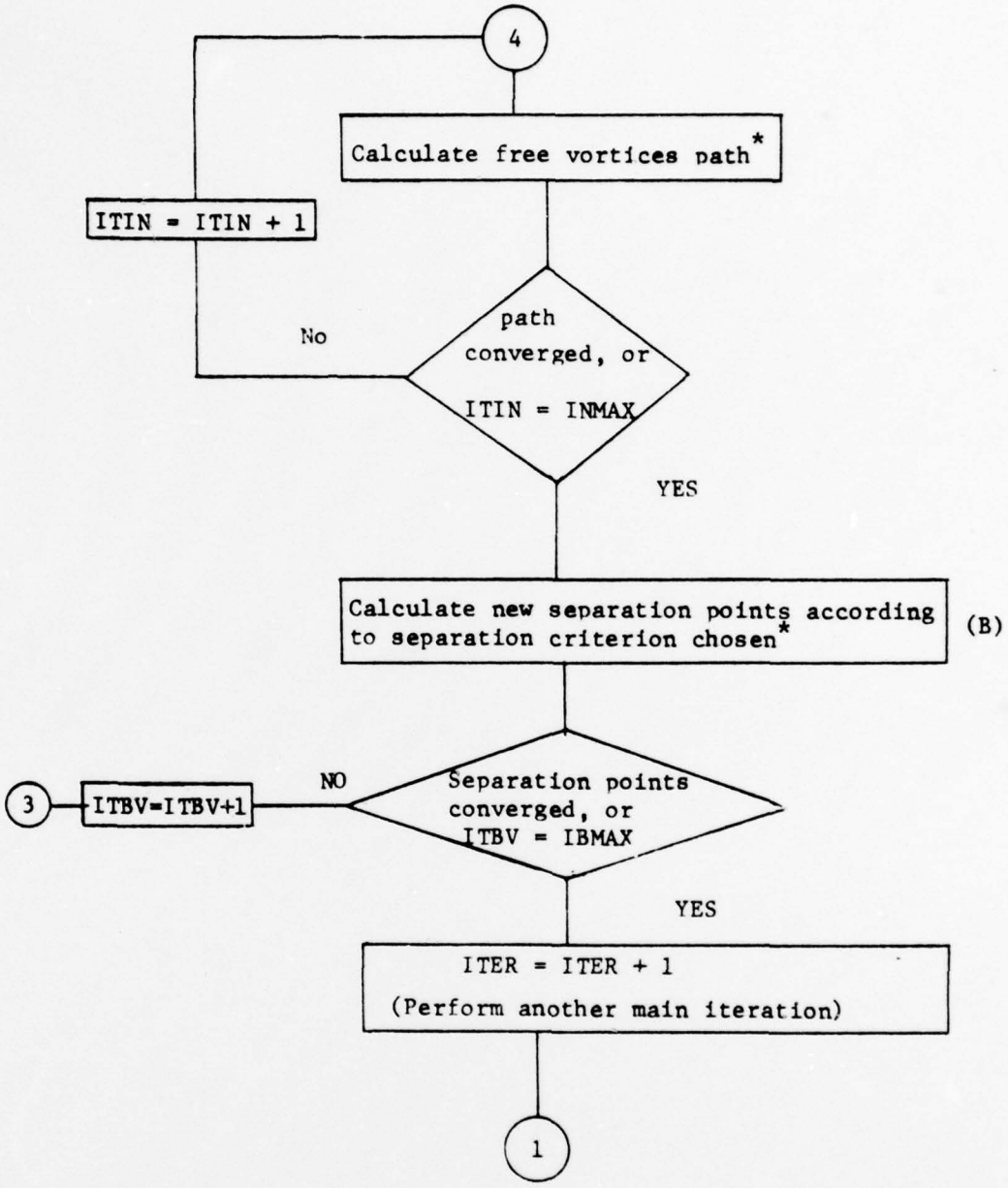

FIG. 23 (CONTINUED).

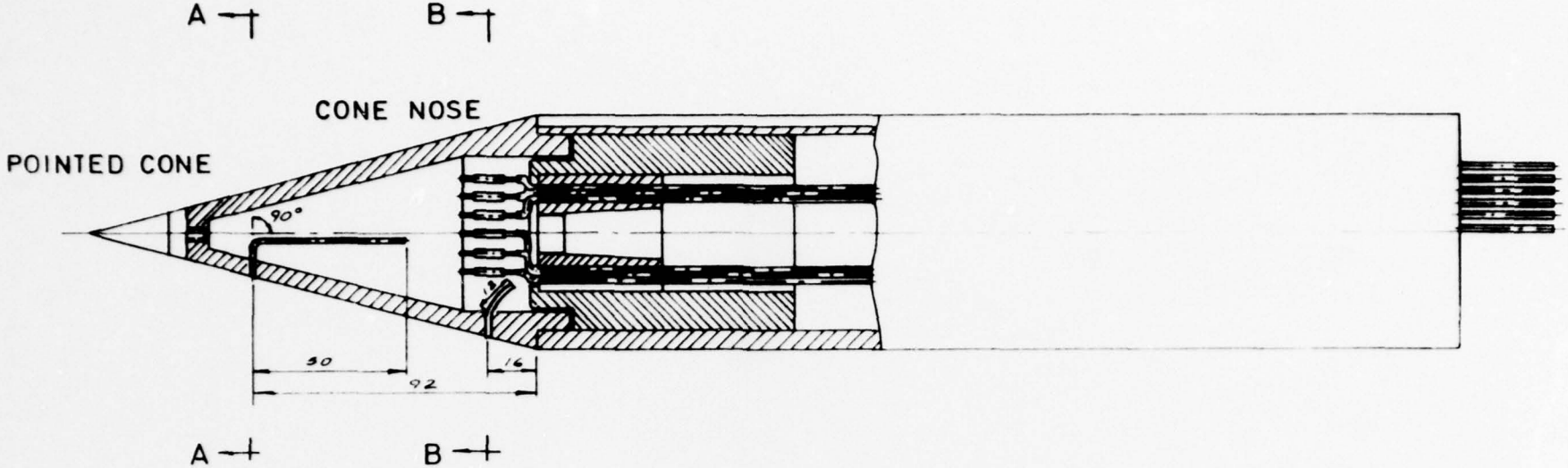

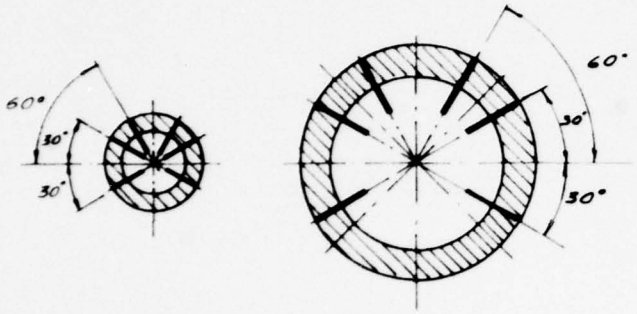

SECTION A-A SECTION B-B

NOSE SHAPES

BLUNT CONE

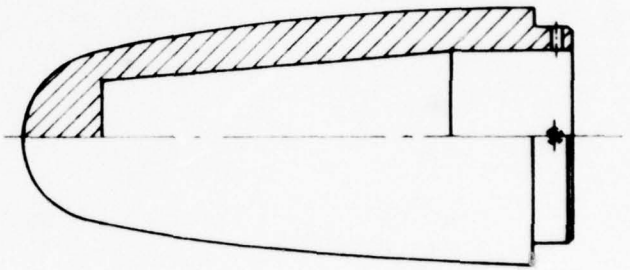

BLUNT OGIVE

FIG.24-WIND TUNNEL MODEL

FIG. 25-FLOW PATTERNS ON THE MODEL

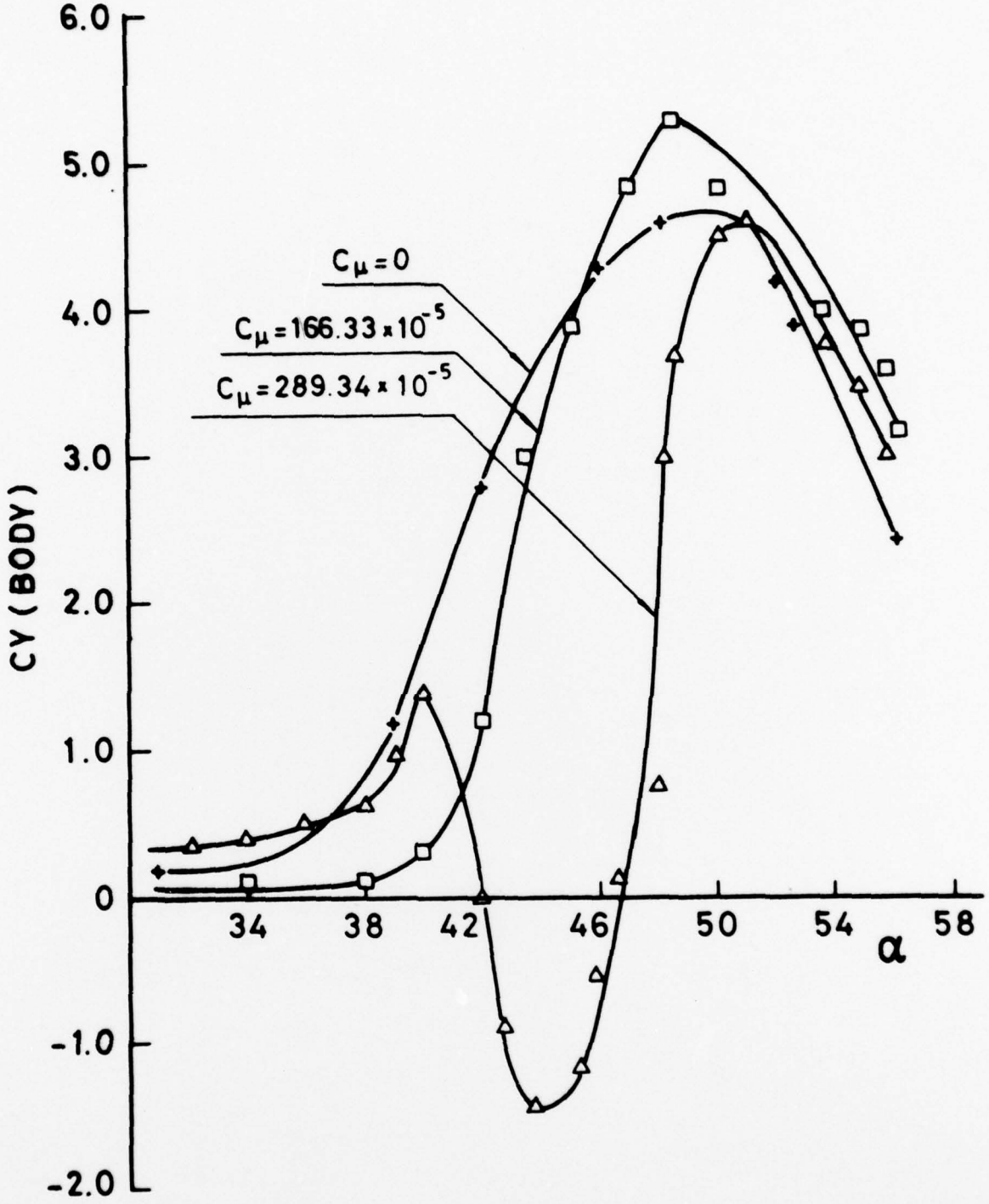

FIG.26- SIDE FORCE COEFFICIENT VERSUS ANGLE OF ATTACK FOR INIJECTION AT STA. I ANGLE +30° (POINTED CONE)

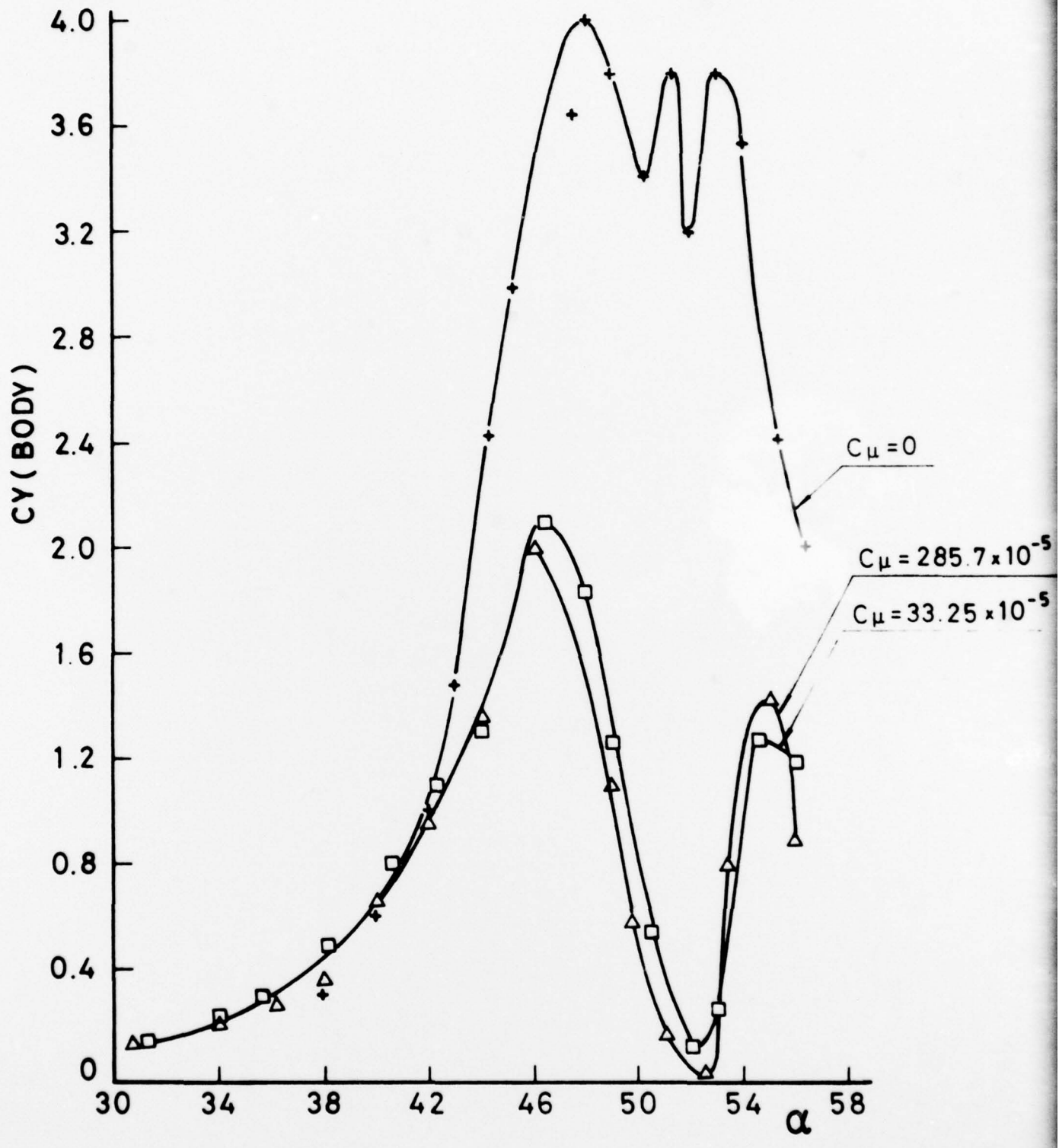

FIG.27-SIDE FORCE COEFFICIENT VERSUS ANGLE OF ATTACK FOR INJECTION AT STA. II ANGLE -30° (POINTED CONE, V= 20 $\frac{m}{sec}$)

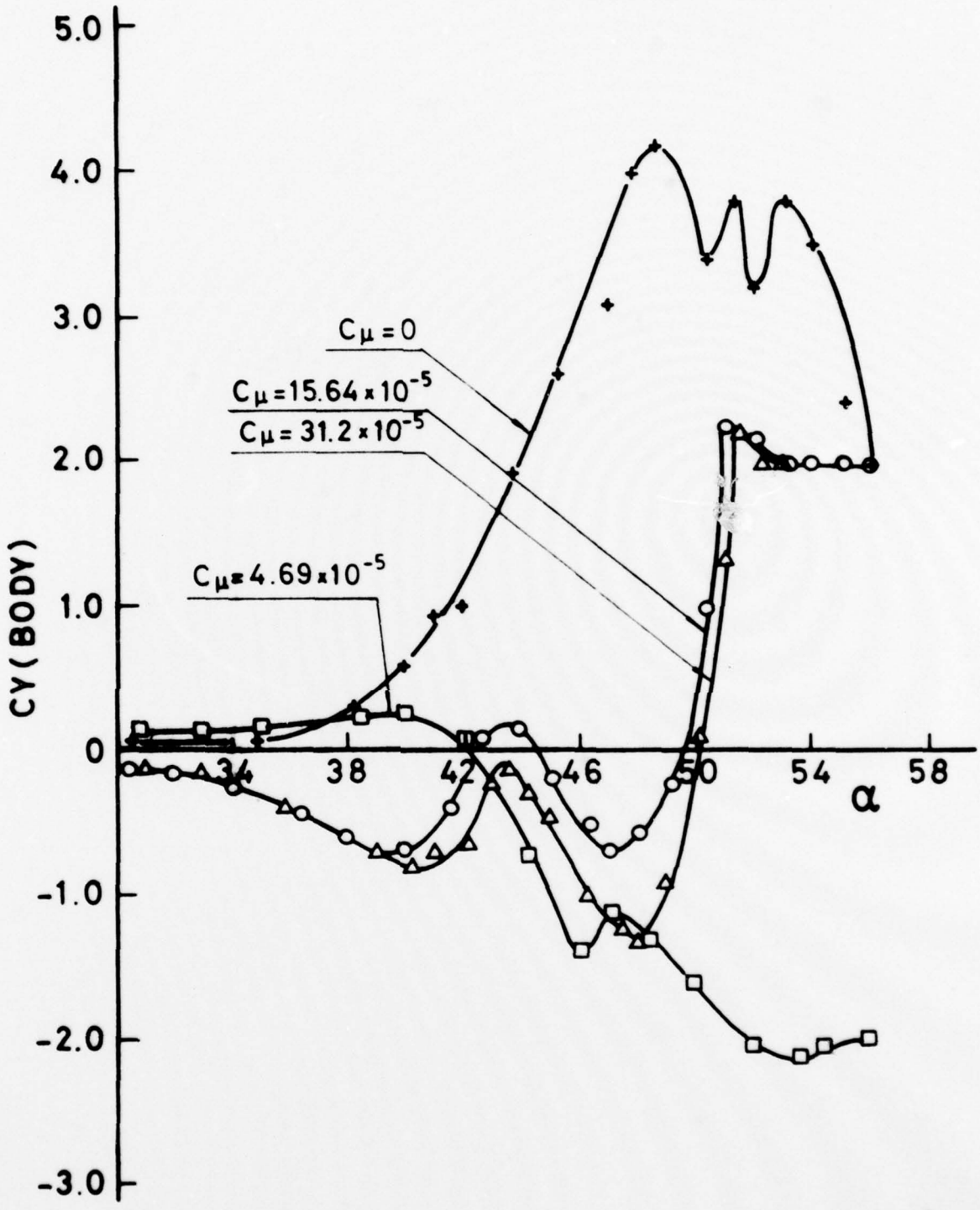

FIG.28-SIDE FORCE COEFFICIENT VERSUS ANGLE OF ATTACK FOR INJECTION AT STA. $\bar{I}$ ANGLE - 30° (POINTED CONE $V = 20 \frac{m}{sec}$)

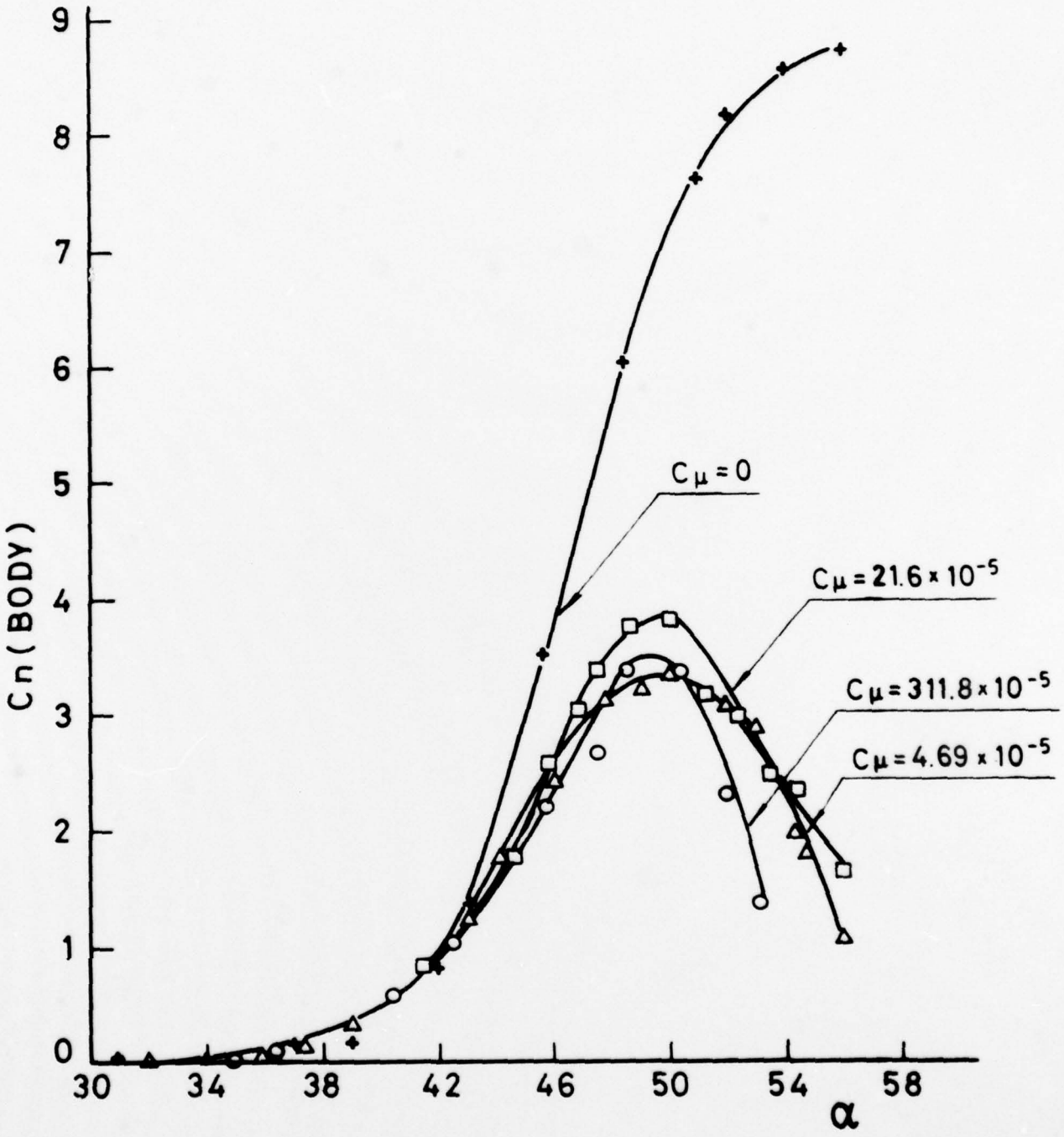

FIG.29- YAWING MOMENT COEFFICIENT VERSUS ANGLE OF ATTACK FOR INJECTION AT STA. I ANGLE -30° (POINTED CONE, V = 20 $\frac{m}{sec}$)

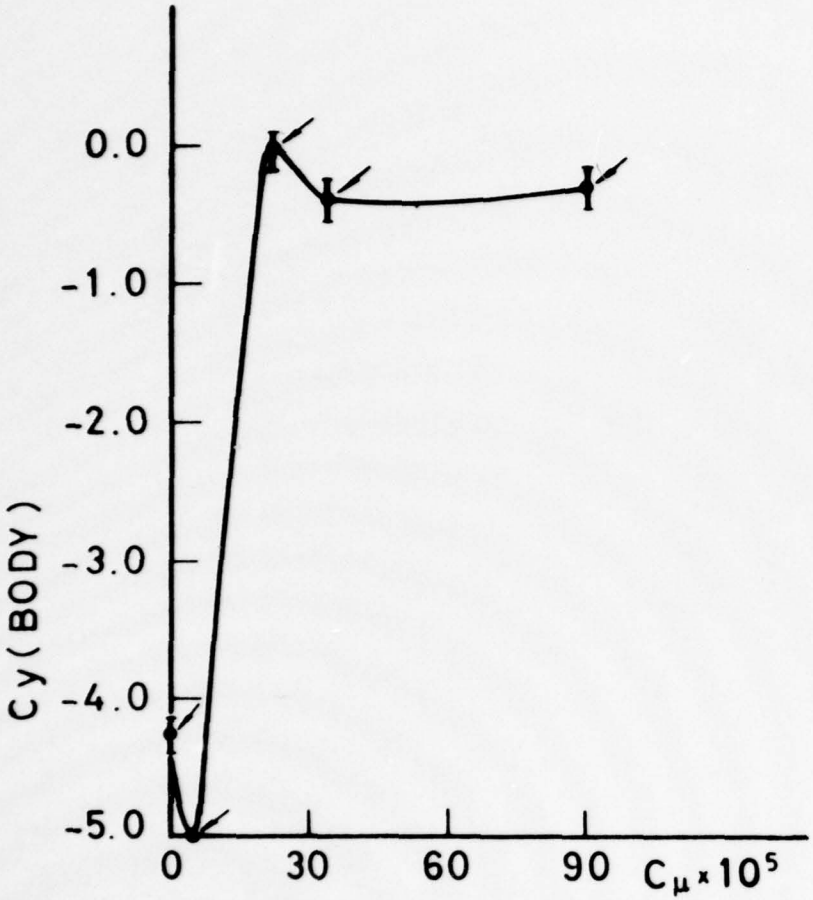

FIG. 30- CHANGE OF SIDE FORCE COEFFICIENT AT 45° ANGLE OF ATTACK FOR INJECTION AT STA. I ANGLE -30°,(POINTED CONE)

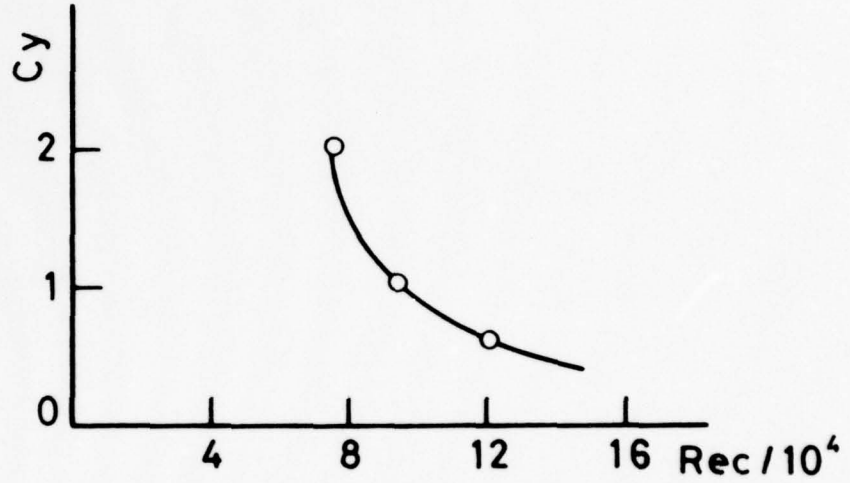

FIG.31-SIDE FORCE COEFFICIENT VERSUS CROSS FLOW REYNOLDS NUMBER AT $\alpha = 45°$ $C\mu = 21.6 \times 10^{-5}$

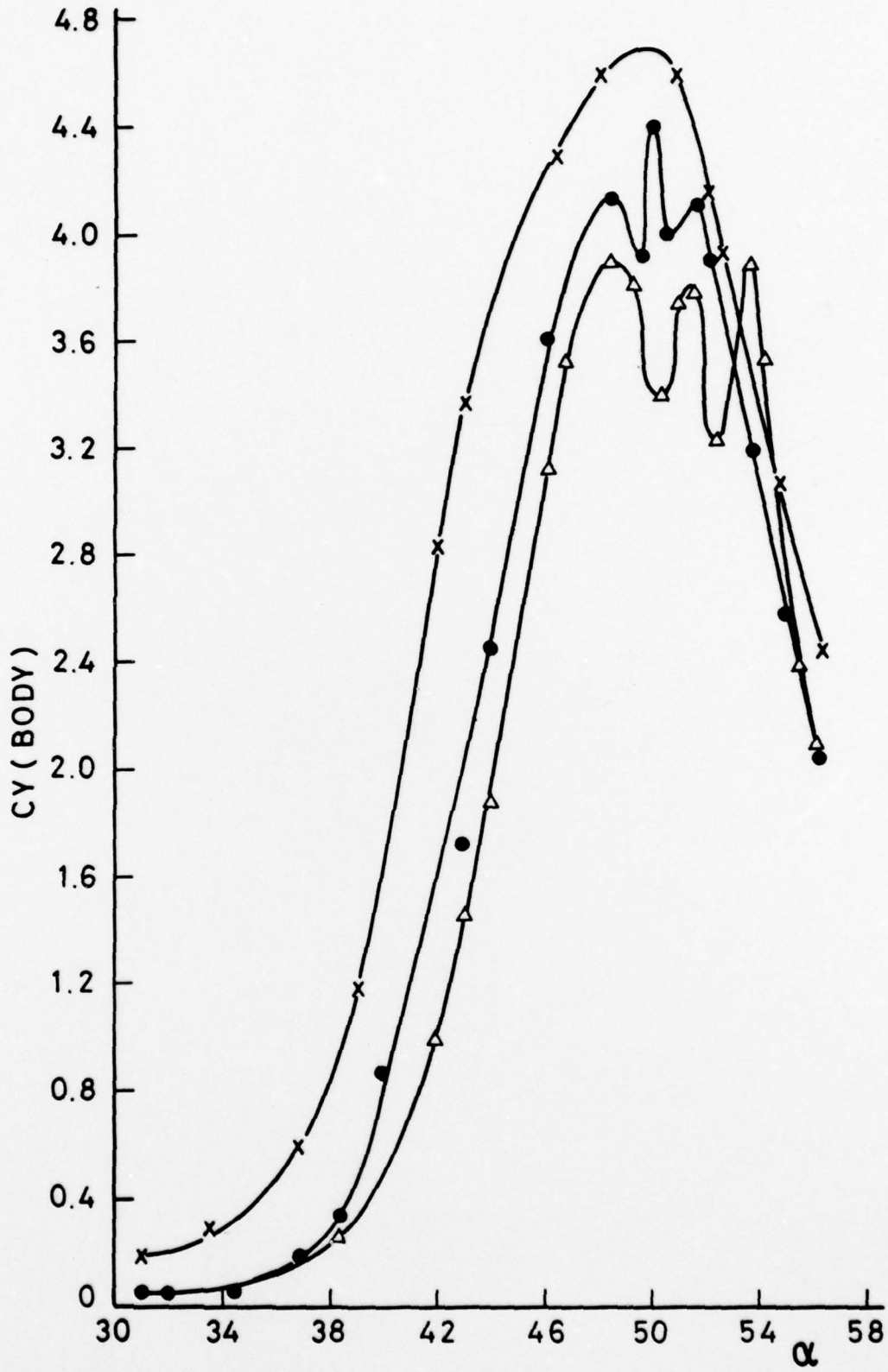

FIG.32-SIDE FORCE COEFFICIENT VERSUS ANGLE OF ATTACK (C_μ=0)

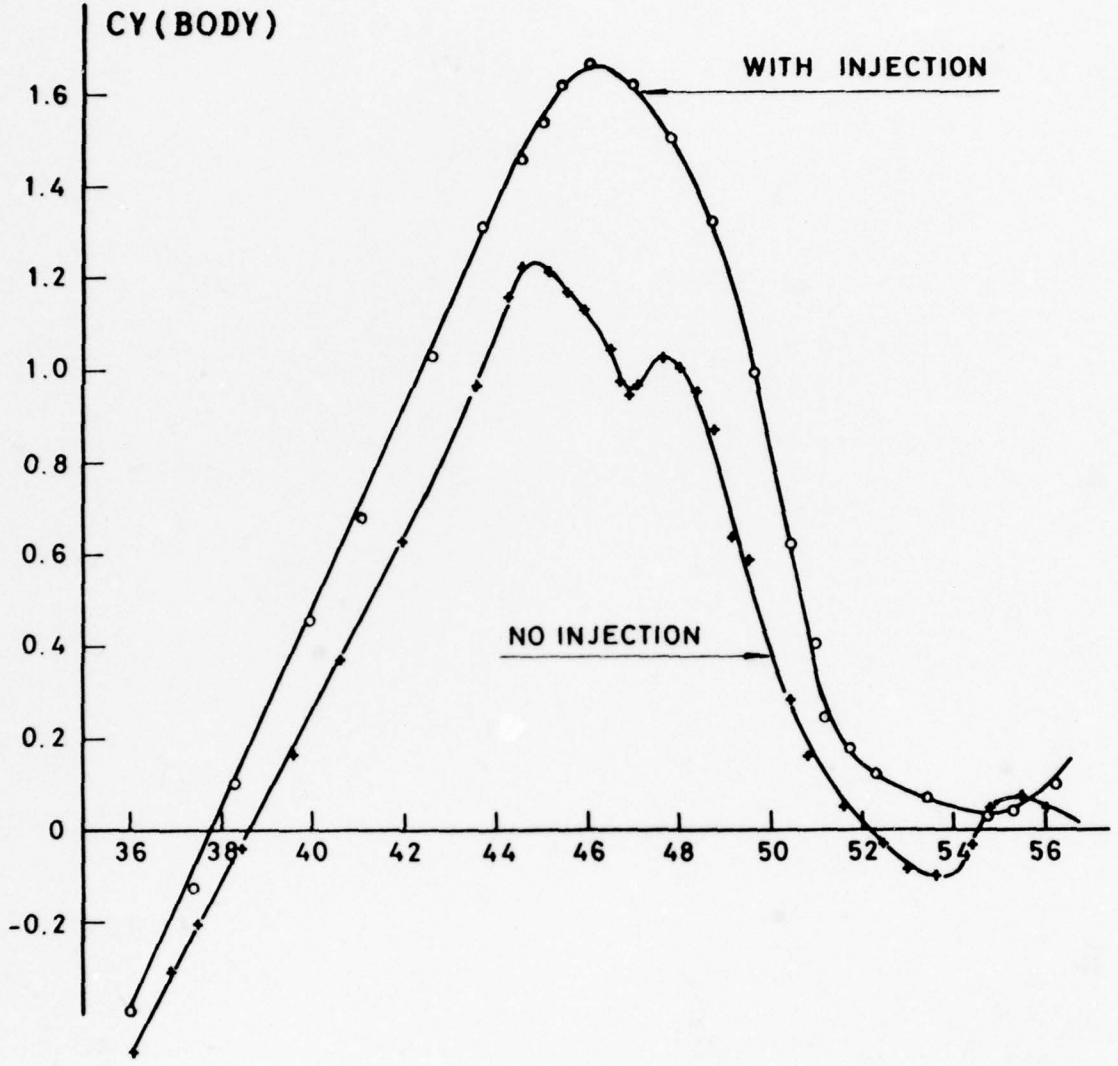

FIG. 33 - SIDE FORCE COEFFICIENT Vs. ANGLE OF ATTACK, AT 0.6 MACH NUMBER $C\mu = 149.4 \times 10^{-7}$

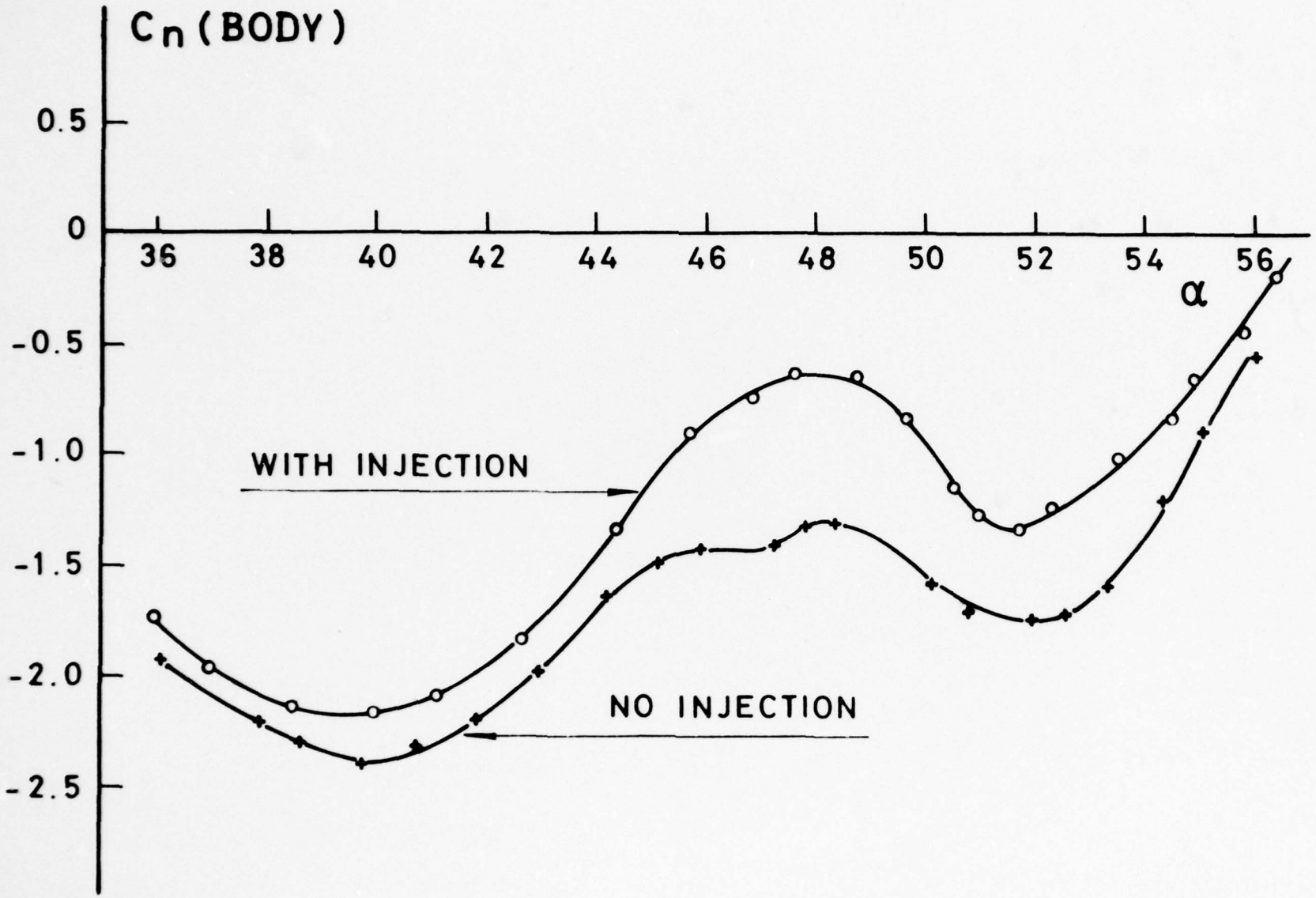

FIG. 34 - YAWING MOMENT COEFFICIENT Vs. ANGLE OF ATTACK, AT 0.6 MACH NUMBER $C_\mu = 149.4 \times 10^{-7}$

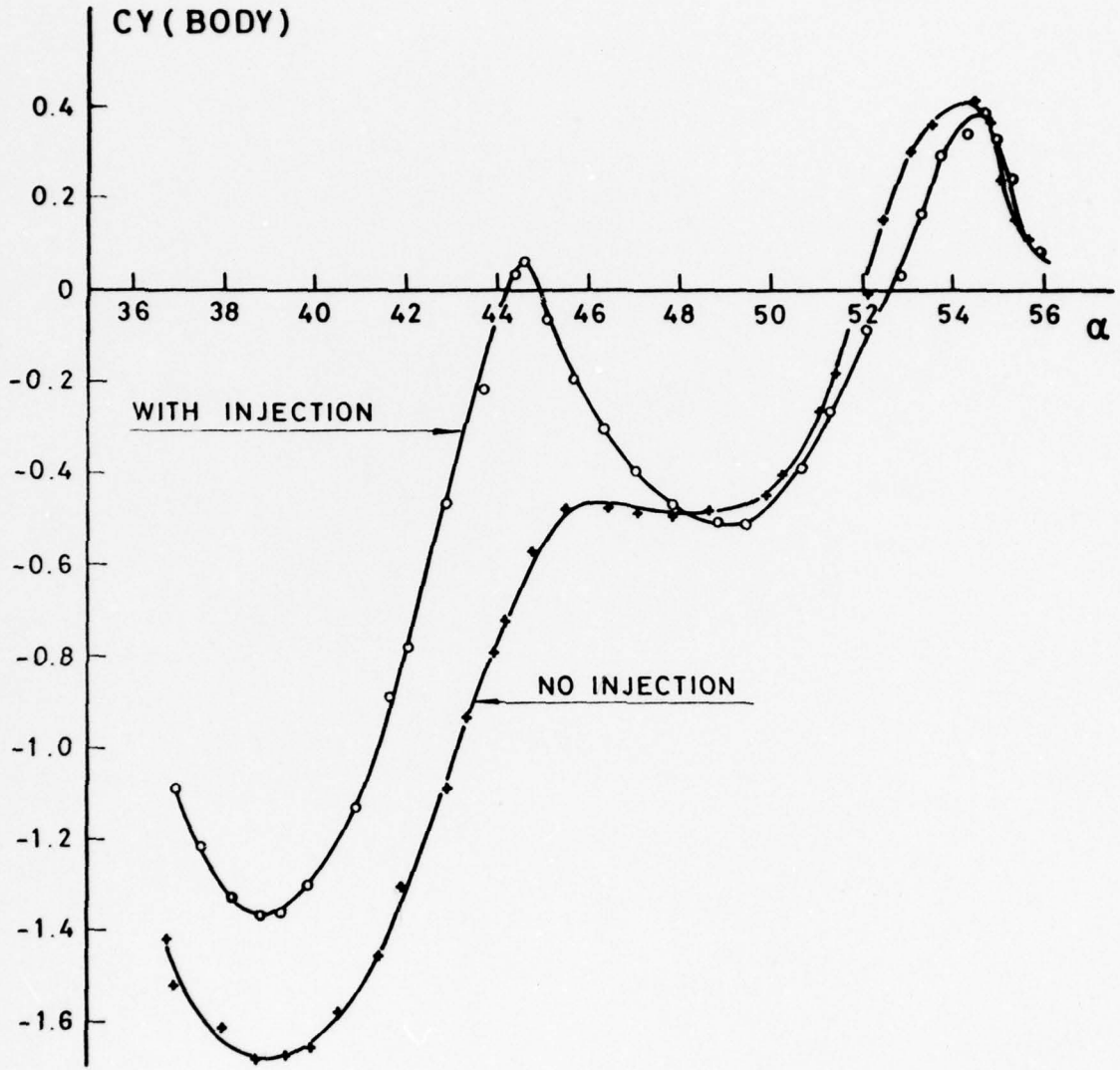

FIG. 35 - SIDE FORCE COEFFICIENT Vs. ANGLE OF ATTACK, AT 0.8 MACH NUMBER $C\mu = 149.4 \times 10^{-7}$

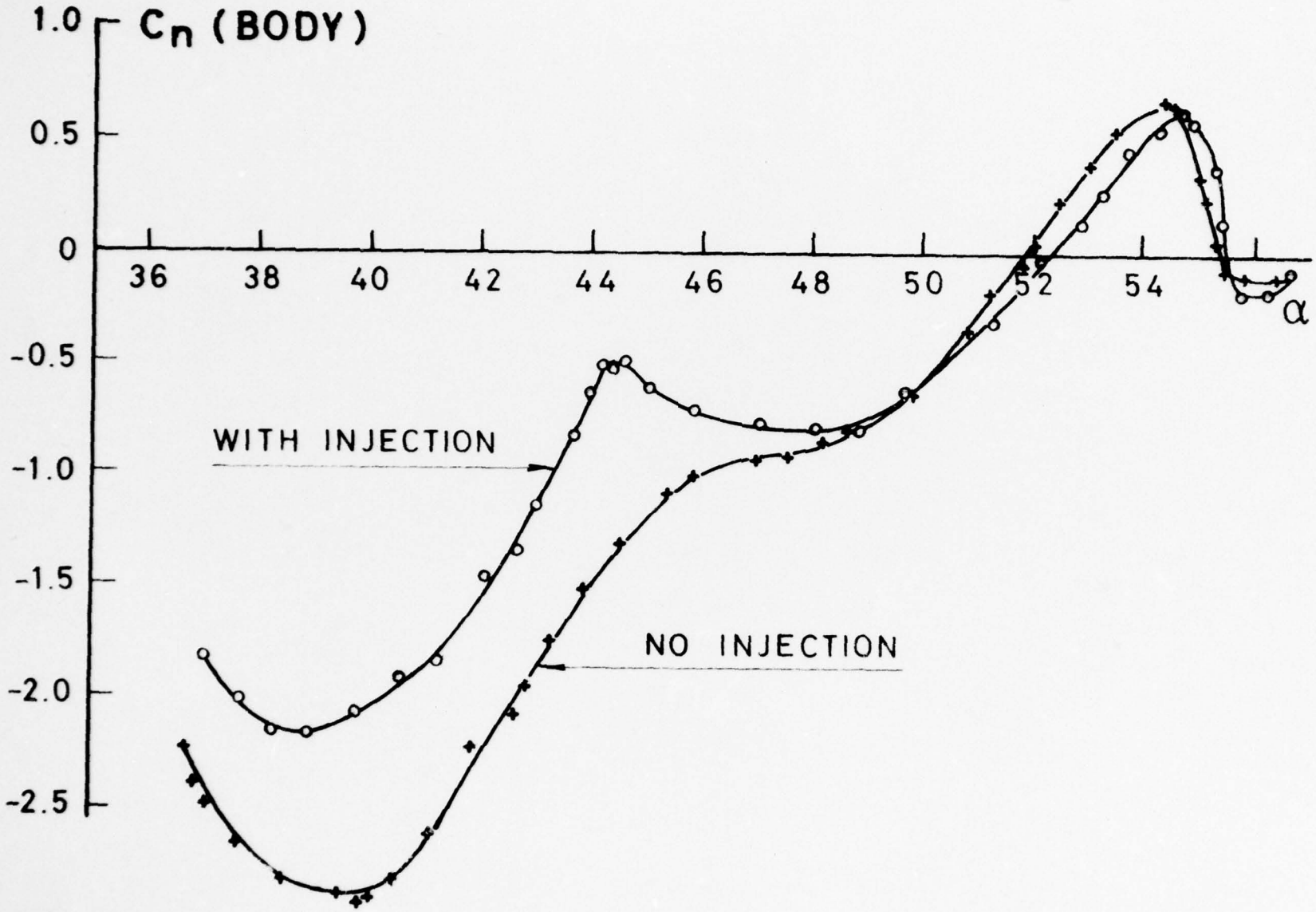

FIG. 36 - YAWING MOMENT COEFFICIENT Vs. ANGLE OF ATTACK, AT 0.8 MACH NUMBER $C_\mu = 84.1 \times 10^{-7}$

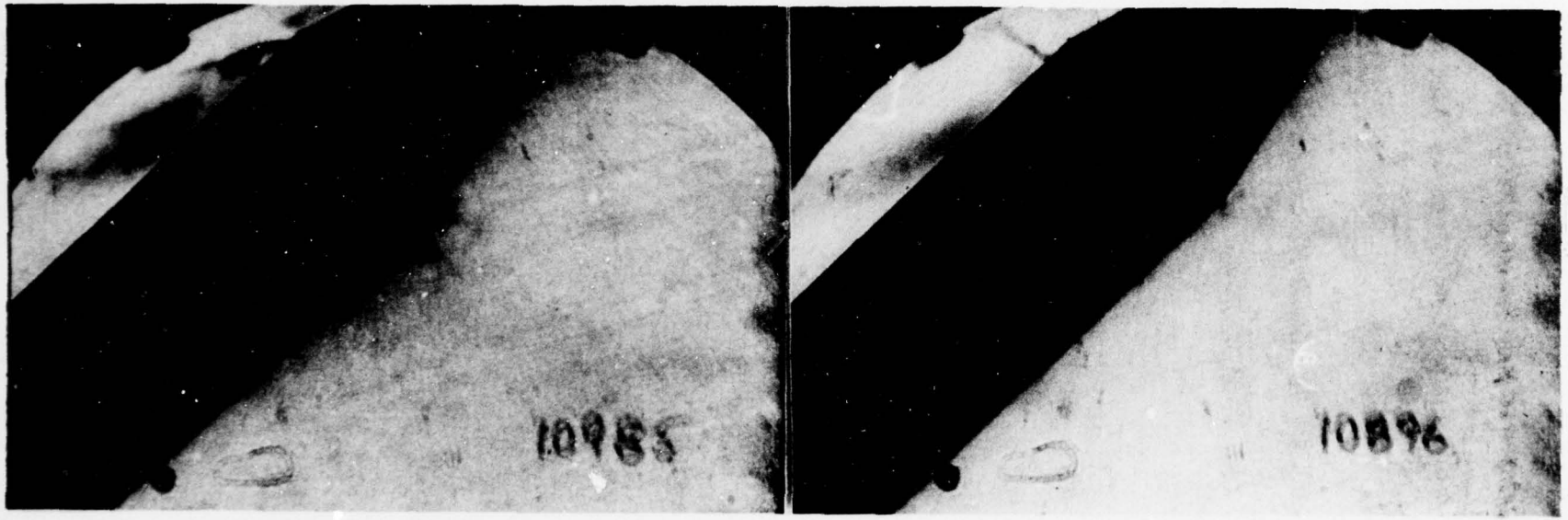

a
NO INJECTION

b
WITH INJECTION

FIG. 37 - SCHLIEREN PHOTOGRAPHS OF THE BODY AT 0.8 MACH NUMBER, $\alpha = 44°$